α-Glucosidase Inhibitors from a *Xylaria feejeensis* Associated with *Hintonia latiflora*

By: José Rivera-Chávez, Mario Figueroa, María del Carmen González, Anthony E. Glenn, and Rachel Mata

Rivera-Chávez, J., Figueroa, M., González, M.D.C., Glenn, A.E., Mata, R. (2015). α-Glucosidase Inhibitors from a *Xylaria feejeensis* Associated with *Hintonia latiflora*. *Journal of Natural Products, 78* (4), pp. 730-735. DOI: 10.1021/np500897y

Abstract:

Two new compounds, pestalotin 4′-*O*-methyl-β-mannopyranoside (**1**) and 3*S*,4*R*-(+)-4-hydroxymellein (**2**), were isolated from an organic extract of a *Xylaria feejeensis*, which was isolated as an endophytic fungus from *Hintonia latiflora.* In addition, the known compounds 3*S*,4*S*-(+)-4-hydroxymellein (**3**), 3*S*-(+)-8-methoxymellein (**4**), and the quinone derivatives 2-hydroxy-5-methoxy-3-methylcyclohexa-2,5-diene-1,4-dione (**5**), 4*S*,5*S*,6*S*-4-hydroxy-3-methoxy-5-methyl-5,6-epoxycyclohex-2-en-1-one (**6**), and 4*R*,5*R*-dihydroxy-3-methoxy-5-methylcyclohexen-2-en-1-one (**7**) were obtained. The structures of **1** and **2** were elucidated using a set of spectroscopic and spectrometric techniques. The absolute configuration of the stereogenic centers of **1** and **2** was determined using ECD spectroscopy combined with time-dependent density functional theory calculations. In the case of **1**, comparison of the experimental and theoretical $^{3}J_{6-7}$ coupling constants provided further evidence for the stereochemical assignments. Compounds **2** and **3** inhibited *Saccharomyces cerevisiae* α-glucosidase (αGHY), with IC_{50} values of 441 ± 23 and 549 ± 2.5 μM, respectively. Their activity was comparable to that of acarbose (IC_{50} = 545 ± 19 μM), used as positive control. Molecular docking predicted that both compounds bind to αGHY in a site different from the catalytic domain, which could imply an allosteric type of inhibition.

Keywords: *Xylaria feejeensis* | *Hintonia latiflora* | type II diabetes mellitus treatments

Article:

Members of the genus *Xylaria* (Xylariaceae), with more than 300 species, are ubiquitous as endophytes in vascular plants.(1) *Xylaria* have received special attention due to their potential as a source of novel secondary metabolites; a recent review showed that more than 180 compounds, including sesquiterpenoids, diterpenoids, diterpene glycosides, triterpene glycosides, steroids, N-containing compounds, pyrone derivatives, and polyketides, have been isolated from this genus.(2) Specifically, from *Xylaria feejeensis*, integric acid,(1) xylaropyrone,(1) and the nonenolide xyolide(3) have been isolated.

The current study was undertaken to address the need for new treatments for type II diabetes mellitus (TIIDM), which according to the International Diabetes Federation is a huge growing health problem worldwide.(4, 5) Thus, as part of our continuing search for new α-glucosidase inhibitors useful for the treatment of TIIDM, we evaluated products **1**–**7** isolated from *X. feejeensis* associated with *Hintonia latiflora* (Sessé et Moc. ex DC.) Bull. (Rubiaceae), a plant widely used as an antidiabetic herbal drug in the context of alternative and complementary medicine in Mexico and Europe.(6)

Results and Discussion

An organic extract from *X. feejeensis* showed moderate inhibition (40% at 250 ppm) when it was tested against α-glucosidase (αGHY). Bioassay-guided fractionation of this extract using different chromatographic procedures led to the isolation of two new natural products, namely, pestalotin 4′-*O*-methyl-β-mannopyranoside (**1**) and 3*S*,4*R*-(+)-4-hydroxymellein (**2**), along with several known compounds, which were identified as 3*S*,4*S*-(+)-4-hydroxymellein (**3**), 3*S*-(+)-8-methoxymellein (**4**), 2-hydroxy-5-methoxy-3-methylcyclohexa-2,5-diene-1,4-dione (**5**), 4*S*,5*S*,6*S*-4-hydroxy-3-methoxy-5-methyl-5,6-epoxycyclohex-2-en-1-one (**6**), and 4*R*,5*R*-dihydroxy-3-methoxy-5-methylcyclohexen-2-en-1-one (**7**).(7-10)

Compound **1** was isolated as a glassy, brown solid. Its molecular formula was deduced to be $C_{18}H_{30}O_9$ by HRESIMS. The IR spectrum displayed absorptions bands for hydroxyl (3399 cm^{-1}) and unsaturated δ-lactone (1691 cm^{-1}) groups. The ^1H and ^{13}C NMR spectra (Table 1) were very similar to those reported for pestalotin analogues(11, 12) except for the presence of signals attributed to a methyl-hexose moiety (δ_H/δ_C 4.64/102.1 H-1′/C-1′; 3.84/72.9 H-2′/C-2′; 3.53/75.3 H-3′/C-3′; 3.31/78.0 H-4′/C-4′; 3.12/77.2 H-5′/C-5′; and 3.67, 3.78/62.5 H-6a′, H6b′/C-6′). This sugar was characterized as 4-*O*-methyl-β-mannopyranosyl on the basis of the coupling pattern observed for H-1′ (δ_H 4.64, d, J = 1.0 Hz), H-2′ (δ_H 3.84, dd, J = 1.0, 3.5 Hz), and H-3′ (δ_H 3.53, dd, J = 3.3 and 9.4 Hz). In addition, the ROESY experiment revealed strong interactions between H-1′, H-2′, H-3′, and H-5′ and between H-3′, H-5′, and H-2′ and the methyl group at C-4′, which were expected for a 4-*O*-methyl-β-mannopyranosyl residue. On the other hand, the strong HMBC interaction between H-1′ (δ_H 4.64) and C-7 (δ_C 80.5) revealed that the sugar unit was attached to the hydroxy group at C-7 through an *O*-glycosidic linkage. Finally, the loss of 176 units from the $[M + H]^+$ ion in the HRESIMS spectrum further supports the presence of a 4-*O*-methyl-β-mannopyranosyl moiety (Figure S2, Supporting Information).

Table 1. NMR Data of 1 in MeOH-*d*$_4$ (^{1}H 500 MHz, ^{13}C 125 MHz)

position	δ_C		δ_H (*J* in *Hz*)	HMBC	COSY	ROESY
2	170.0	C				
3	90.1	CH	5.14 d (1.4)	2, 4, 5		
4	176.2	C				
5	30.0	CH_2	a 2.35 dd (3.8, 17.1)	3, 4	6	
			b 2.67 ddd (1.0, 12.5, 16.7)	4, 6, 7		
6	79.3	CH	4.45 ddd (3.9, 5.5, 12.7)	7	5, 7	
7	80.5	CH	3.84 m	5a, 1′	6	
8	31.5	CH_2	1.58 m	7	7	
9	28.1	CH_2	1.44 tdd (6.9, 14.8, 19.4)		8	
10	23.7	CH_2	1.27 m		9	
11	14.3	CH_3	0.89 t (7.3)	9, 10	10	

position	δ_C		δ_H (*J* in *Hz*)	HMBC	COSY	ROESY
4-OMe	57.1	CH_3	3.75 s	4		
1′	102.1	CH	4.64 d (1.0)	7, 2′		2′, 3′, 5′
2′	72.9	CH	3.84 dd (1.0, 3.5)		3′	
3′	75.3	CH	3.53 dd (3.3, 9.4)		2′, 4′	2′, 5′
4′	78.0	CH	3.31 t (9.5)		3′, 5′	
5′	77.2	CH	3.12 ddd (2.0, 4.3, 9.6)		4′, 6′	3′, 5′
6′	62.5	CH_2	a 3.67 dd (4.4, 11.7)			
			b 3.78 dd (2.0, 11.9)			
4′-OMe	61.0	CH_3	3.50 s			

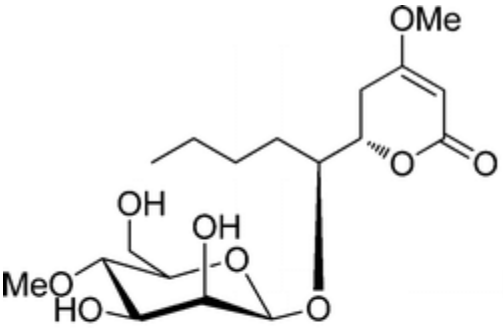

1a

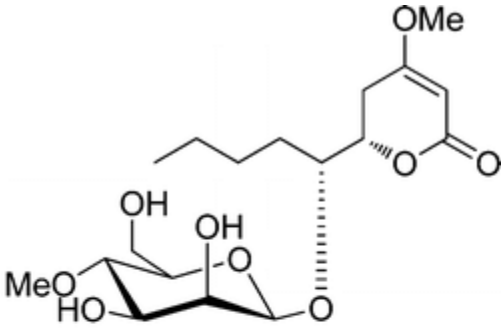

1b

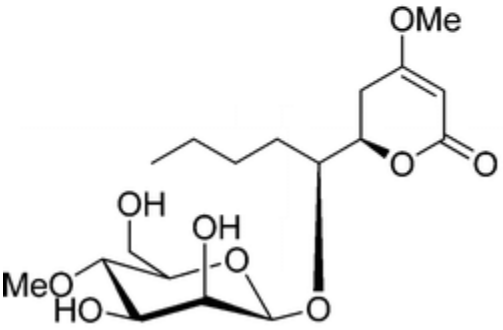

1c

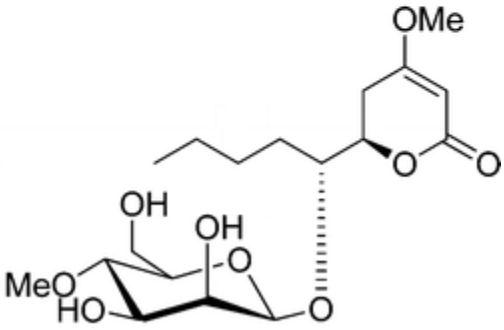

1d

In order to establish the absolute configuration at C-6, the ECD spectrum of **1** was recorded and compared with density functional theory (DFT)-calculated spectra for diastereoisomers 6*S*,7*S*, 6*S*,7*R*, 6*R*,7*S*, and 6*R*,7*R* of **1** (**1a**–**1d**, respectively). Initially the structure of each diastereoisomer was minimized; subsequently, a conformational search was performed using a Monte Carlo protocol. All conformers for each diasteroisomer, within a 3 kcal/mol window, were selected and reoptimized using DFT calculations at the B3LYP/DGDZVP level. After optimization, theoretical ECD spectra of each conformer of **1a**–**1d** were calculated using time-dependent density functional theory (TDDFT) at the same level.(13) The calculated ECD spectrum for distereoisomer **1a** showed an excellent fit with the experimental plot of **1**, which displayed positive and negative Cotton effects at 230 and 260 nm, respectively (Figure 1). Considering these results, diastereoisomers **1c** and **1d** were automatically ruled out. The calculated ECD for **1b** showed two positive Cotton effects, leaving diasteroisomer **1a** as the best structural candidate for compound **1**. Hence, the absolute configuration at C-6 was established as *S.* Next, to ensure the absolute configuration at C-7, the calculated $^3J_{6–7}$, $^3J_{5pro\mathit{R}\text{-}6}$, and $^3J_{5pro\mathit{S}\text{-}6}$ (obtained from theoretical calculations using DFT at the B3LYP/DGDZVP level)(14a, 14b) vs

the experimental (obtained from the ^{1}H NMR using double resonance experiments by selective irradiation at δ_H 2.35 and 2.67 ppm) values were compared. The analysis was undertaken only for diastereoisomers **1a** and **1b**, which possesses an *S* configuration at C-6. The smallest rmsd (0.64) between calculated and experimental $^{3}J_{6-7}$ values (Table 2) obtained for diasteroisomer **1a** confirmed the *S* absolute configuration at C-7. For **1b**, the calculated $^{3}J_{6-7}$ showed noticeable differences (rmsd = 5.03) from the experimental values, ruling out this structure. The coexistence of **1** and d-mannitol suggests that the methyl-β-mannopyranoside residue belongs to the d-series. Unfortunately, the lack of a suitable standard precludes unambiguous assignment of the sugar configuration. Thus, compound **1** was characterized as 6*S*,7*S*-(−)-pestalotin 4′-*O*-methyl-β-mannopyranoside.

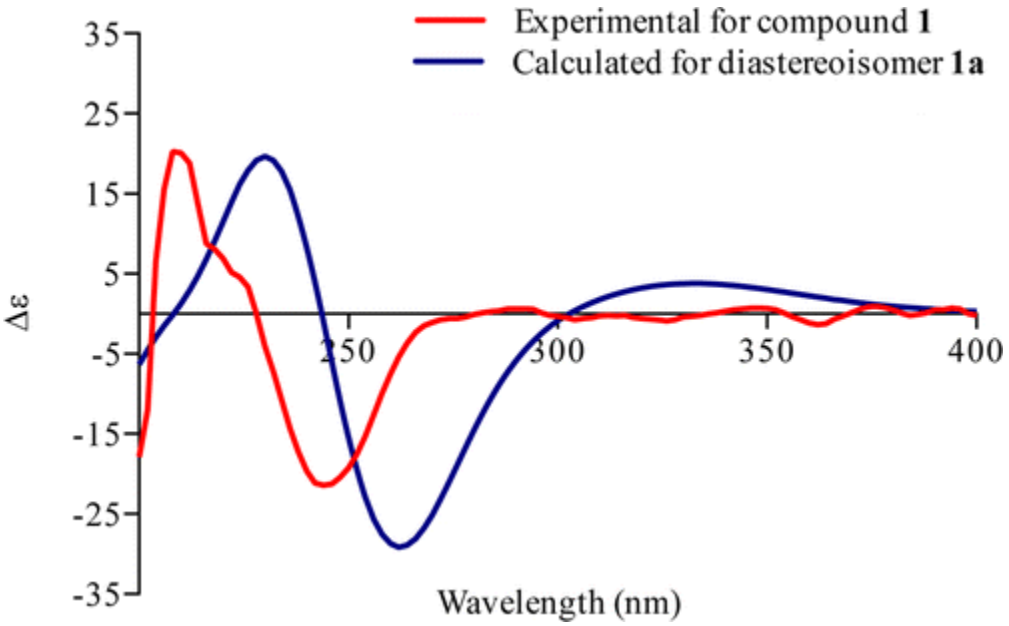

Figure 1. Comparison of experimental and calculated ECD spectra of **1** (red line) and **1a** (blue line).

Table 2. DFT-Calculated and Experimental ^{1}H–^{1}H Coupling Constants of 1

		calculated coupling constants[a]	
$^{3}J_{H-H}$	experimental	1a	1b
J_{6-7}	5.5	6.5[b]	7.0[b]
$J_{5proR-6}$	3.8	3.5	5.9
$J_{5proS-6}$	12.6	13.0	4.3
rmsd		0.64	5.03

[a] Coupling constants are expressed in Hz. Theoretical coupling constants were calculated at the B3LYP/DGTZVP level of theory. Coupling constants were Boltzman-weighted using $\sum_i J^i \times P^i$, where J^i is the coupling constant value for each conformer and P^i is the population of the conformation.
[b] The averaged coupling constants were scaled with the factor $f_{H(sp3)-H(sp3)}$ = 0.910.(14b)

Compound **2** was obtained as an optically active, yellow powder ($[\alpha]_D$ = +32). Its UV and NMR (Table 3) spectra showed close relationship with those of 3*S*,4*S*-(+)-4-hydroxymellein (**3**).(7) Key differences between **2** and **3** were the chemical shift values and splitting patterns of H-3 and H-4. The signals of the oxygenated methines at δ_H/δ_C 4.72, qd, *J* = 2.1, 6.6 Hz, H-3/79.9 and δ_H/δ_C 4.55, d, *J* = 2.1 Hz, H-4/67.6 in **2** were replaced by a multiplet centered at δ_H 4.56

(δ_C 81.6, C-3 and 69.5, C-4) in **3**. This information revealed that these compounds differed in the absolute configuration at C-3 and/or C-4 (Figures S11,12 and S16,17).

Table 3. NMR Data of 2 in MeOH-*d*$_4$ (^{1}H 400 MHz, ^{13}C 100 MHz)

position	δ_C		δ_H (*J* in Hz)	HMBC	COSY
1	171.0	C			
3	79.9	CH	4.72 qd (2.1, 6.6)		4
4	67.6	CH	4.55 d (2.1)	4a, 5, 8a	3
4a	143.1	C			
5	119.8	CH	6.96 d (8.4)	4, 6	
6	137.7	CH	7.56 dd (7.4, 8.5)	5, 7	
7	118.5	CH	6.99 d (7.4)	6, 8	
8	162.9	C			
8a	108.4	C			
9	16.4	CH_3	1.52 d (6.6)	3, 4	

The absolute configuration at the stereogenic centers of **2** and **3** was established by comparing experimentally measured ECD spectra and those calculated by TDDFT using the same protocol described for compound **1**. The chiroptical properties of the dihydroisocoumarin benzoic ester chromophore were systematically investigated; it was shown that the sign of the Cotton effect of the ester n→π* transition at 260 nm, which is independent of the substitution pattern of the aromatic ring, can be used to establish the absolute configuration at C-3.(15) The ECD-calculated spectrum obtained for diastereoisomer 3*S*,4*R*-**2** (**2c**) (Figure S21) was in agreement with the experimental data. In both cases one negative (316 nm) and a positive Cotton effect (255 nm), assignable to the n → π* transition, were observed (Figure 2). Thus, the absolute configuration at C-3 was established as *S*. On the other hand, the absolute configuration at C-4 was determined by comparison of the experimental ECD spectra of **2** and **3**, which are mirror images of each other between 200 and 260 nm, confirming the opposite configuration of the hydroxy group at this position (Figure 2).

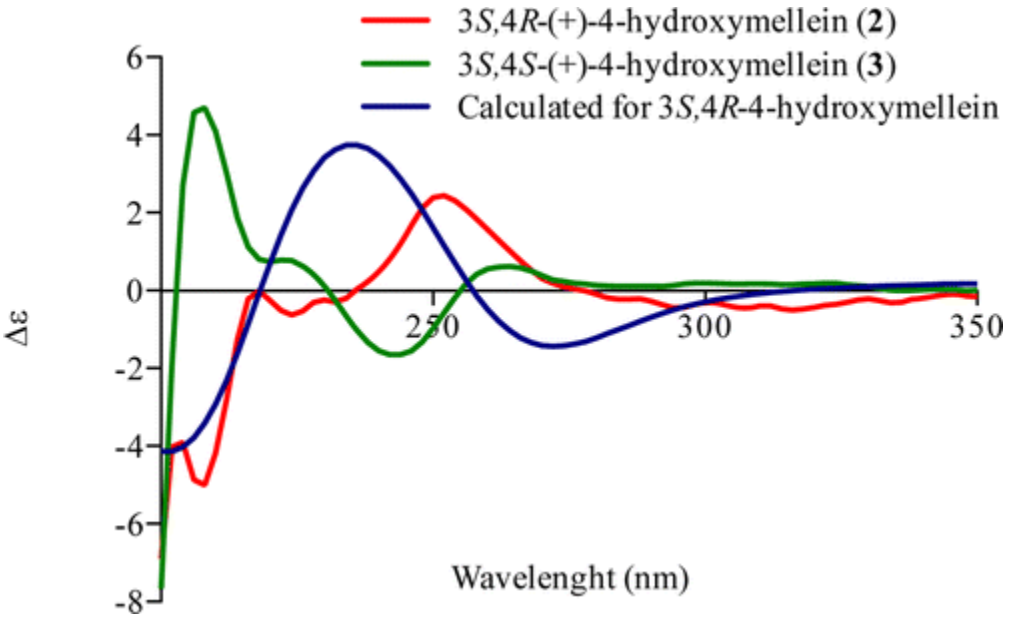

Figure 2. Comparison of experimental ECD spectra of **2** (red line) and **3** (green line) and the calculated ECD spectrum for diatereoisomer 3*S*,4*R* of 4-hydroxymellein (blue line).

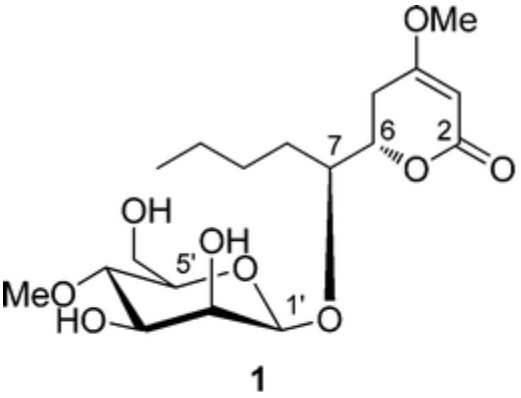

1

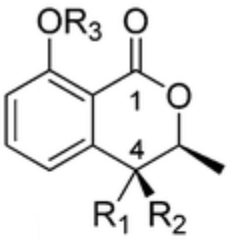

2 R_1 = OH, R_2 = R_3 = H
3 R_1 = R_3 = H, R_2 = OH
4 R_1 = R_2 = H, R_3 = OMe

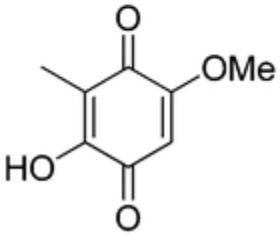

5

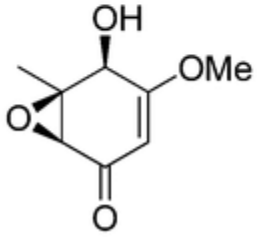

6

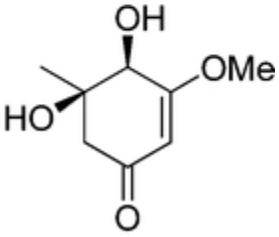

7

The isolates **1**–**7** were tested to determine their effect against αGHY using a well-known spectrophotometric procedure.(16, 17) Only compounds **2** and **3** inhibited the activity of the enzyme in a concentration-dependent manner, with IC_{50} values of 441 ± 23 and 549 ± 2.5 μM, respectively. The inhibitory action of these compounds was similar to that of acarbose (IC_{50} = 545 ± 19 μM), used as positive control. Therefore, on the basis of our previous experiences, these isocoumarins might exert antihyperglycemic action *in vivo*.(6, 17) The results also indicated that the absolute configuration at C-4 has little impact on the enzymatic inhibitory activity.

To assess the putative binding mode of compounds **2** and **3** with αGHY, a molecular docking study was carried out using the crystal structure of αGHY (PDB code: 3A4A) in complex with its competitive inhibitor maltose.(18, 19) The docking protocol was validated reproducing the binding mode of natural ligands maltose and isomaltose into the enzyme.(17) The docking results predicted that **2** and **3** bind in a different place to the catalytic domain of αGHY. The binding site for these compounds was found to be composed by Leu-561, Glu-562, Phe-563, Gly-564, Tyr-566, Pro-567, Lys-568, and Val-571. The main interactions were π-cationic, hydrophobic, and hydrogen bonds between Pro-567 and the hydroxy group at C-4 in **2** and **3** and between Lys-568 and the hydroxy group at C-8 in **2** and the carbonyl group at C-1 in **3** (Figure 3B and C). The results for acarbose are also included for comparative purposes (Figure 3A).

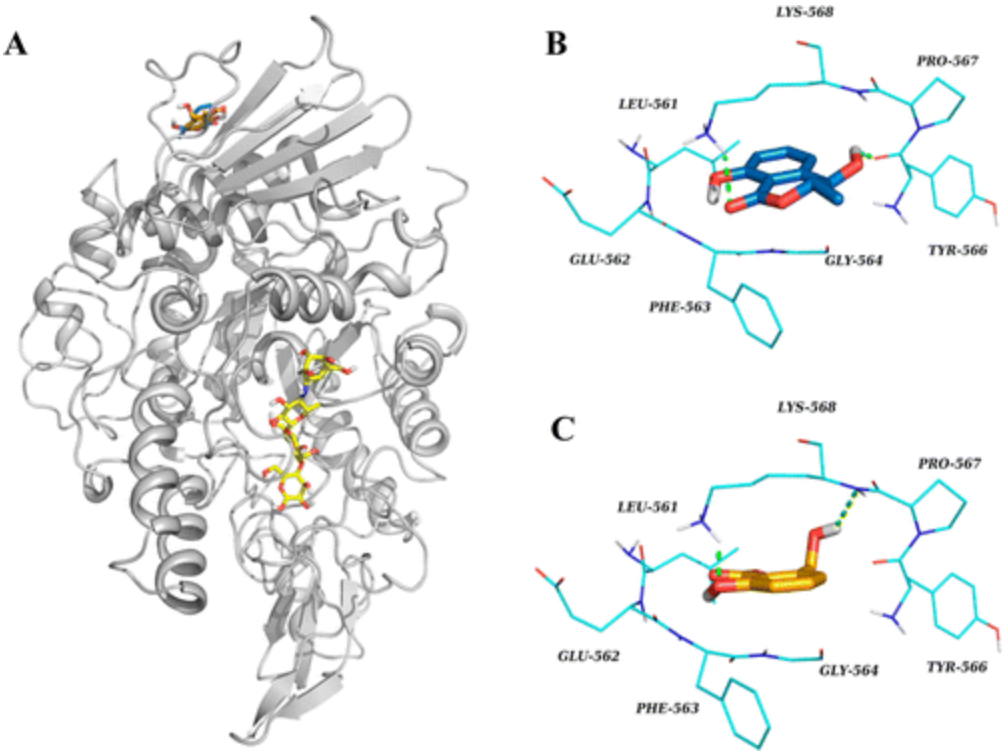

Figure 3. (A) Structural model of the complex 3*S*,4*R*-(+)-4-hydroxymellein (**2**) (blue sticks)-αGHY, 3*S*,4*S*-(+)-4-hydroxymellein (**3**) (orange sticks)-αGHY, and acarbose (yellow sticks)-αGHY. 3D representation of the interaction between (B) **2** and (C) **3** and αGHY, in the binding site predicted. Graphics generated with PyMol.

Experimental Section

General Experimental Procedures

IR spectra were obtained using a PerkinElmer 400 FT-IR spectrophotometer. NMR spectra including HSQC, HMBC, COSY, and ROESY were recorded in MeOH-d_4 in a JEOL-ECA 500 spectrometer at 500 (^{1}H) and 125 MHz (^{13}C) or a Varian Inova 300 at 300 (^{1}H) and 75 MHz (^{13}C); chemical shifts were recorded as δ values. ECD spectra were recorded on an Aviv 202-01 spectrophotometer in MeOH. HRESIMS were recorded on a Thermo Scientific LTQ Orbitrap XL hybrid FTMS (Fourier transform mass spectrometer). Data were collected in both positive and negative ionization modes via a liquid chromatographic/autosampler system that consisted of an Acquity UPLC system. Analytical and preparative HPLC analyses were performed in a Waters system equipped with a 2535 pump and a 2998 photodiode array detector. Control of equipment, data acquisition, processing, and management of chromatographic output were performed by the Empower 3 software (Waters). For analytical, semipreparative, and preparative HPLC, Gemini (C_{18}, 5 µm, 4.6 × 250 mm, Phenomenex), Symmetry (C_{18}, 5 µm, 7.8 × 300 mm, Waters), and Gemini (C_{18}, 5 µm, 21.1 × 250 mm) columns, respectively, were used. Column chromatography (CC) was carried out on Sephadex LH-20 (Sigma-Aldrich-Fluka) or silica gel 60 (70–230 mesh, Merck). Thin-layer chromatography analysis was carried out on silica gel 60 F_{254} plates (Merck) using ceric sulfate (10%) solution in H_2SO_4 as color reagent.

Plant Material

Hintonia latiflora leaves were collected and identified by Sol Cristians-Niizawa in Huetamo (18°31.709′ N, 101°4.692′ W; 221 masl), State of Michoacán, México, in July 2010. A voucher specimen (131,316) was deposited at the Herbarium of the School of Sciences (FCME), UNAM, Mexico City.

Fungus Isolation and Identification

The endophytic fungus *X. feejeensis* was isolated from selected mature leaves of *H. latiflora.* To kill the epiphytic fungi, an efficient protocol for surface sterilization was applied.(20) Complete intact leaves were immersed in 75% EtOH (1 min), 3.4% aqueous sodium hypochlorite solution (10 min), and 75% EtOH (1 min); afterward the sterilized leaves were rinsed with sterilized distilled H_2O and dried with sterile absorbent paper. Sterilized leaves were cut into 5 × 5 mm segments and deposited on a Petri dish (3 to 5 pieces per plate) containing PDA (potato-dextrose agar; Difco), streptomycin sulfate (4 μg/mL), and cyclosporine A (5 μg/mL). The pure fungal strain was obtained after serial transfers on PDA and was deposited in the fungal collections of the Herbario Nacional de Mexico (MEXU) and GenBank [28S rRNA/internal transcribed spacer (ITS) region] under the accession numbers MEXU 27555 and KM192122/KM192123, respectively. Nucleotide BLAST analysis of the 28S rRNA gene sequence from the *H. latiflora* endophyte identified *X. feejeensis* (accession JQ862606) among the top matches, having high coverage (94%) and percent identity (99%) (Figure S22). On the other hand, BLAST analysis of the ITS region was very supportive of it being an isolate of *X. feejeensis.* Most accessions among the top matches were from this species, with accession HM992808 having 94% coverage and 100% identity (Figure S23).

Fermentation, Extraction, and Isolation

The endophytic fungus *X. feejeensis* was cultured at room temperature in two Fernbach flasks containing 200 g of rice and 400 mL of water, which were inoculated using seed cultures grown in the PDB media and incubated at room temperature for 8 days at 200 rpm. After 30 days of fungal growth, the culture media was extracted exhaustively with 1:1 CH_2Cl_2–MeOH (3 × 2 L), and the resulting extract was evaporated *in vacuo* to yield 4.0 g of a brown solid residue. Part of this extract (3.5 g) was resuspended in a 1:1 mix of MeCN–MeOH and subjected to a partition process using hexane. From the MeCN–MeOH fraction precipitated 300 mg of d-mannitol ($[\alpha]_D$ = +24 in water), which was identical to an authentic sample. The mother liquor of the MeCN–MeOH fraction was concentrated *in vacuo* to yield 2.8 g of a dark red solid. This extract was fractionated by CC on silica gel, eluting with gradient of hexane–CH_2Cl_2 (100:0 → 0:100) and CH_2Cl_2–MeOH (10:0 → 5:5). All fractions were monitored by thin-layer chromatography, and fractions with similar patterns were combined to yield six primary fractions (F_I–F_{VI}). Resolution of fraction F_{VI} (700 mg) by semipreparative reversed-phase HPLC (Symmetry 7.8 × 300 mm) using an isocratic mixture as mobile phase (30% MeCN in water, 3.0 mL/min) led to the isolation of pestalotin 4′-*O*-methyl-β-mannopyranoside (**1**, 4.0 mg). Resolution of F_{III} (200 mg) by preparative-phase HPLC (Gemini 21.1 × 250 mm) using a gradient of CH_3CN–0.1% aqueous formic acid (hold for 3.0 min, 0:100; 3.0–13.0 min, 50:50; and hold for 7 min) led to the isolation of **2** (3.0 mg), **3** (1.9 mg), and **4** (3.2 mg). Resolution of F_V (150 mg) by preparative

reversed-phase HPLC using a gradient of CH_3CN–0.1% aqueous formic acid (hold for 5.0 min, 10:90; 5.0–22.0 min, 100:0; and hold for 5 min) led to the isolation of **5** (5.0 mg), **6** (28.5 mg), and **7** (13.2 mg).

Pestalotin 4′-*O*-methyl-β-mannopyranoside (1):

glassy, brown solid; $[\alpha]_D$ −49.0 (*c* 0.1, MeOH); ECD (MeOH) λ_{max} ($\Delta\varepsilon$) 210 (20.28) and 242 nm (−21.17); ^1H and ^{13}C NMR data in Table 1; HRESIMS *m*/*z* 391.1944 $[M + H]^+$ (calcd for $C_{18}H_{31}O_9$, 391.1963).

3*S*,4*R*-(+)-4-Hydroxymellein (2):

yellow powder; $[\alpha]_D$ +32.0 (*c* 0.1, MeOH); UV (MeOH) λ_{max} [log(ε/M^{-1} cm^{-1})] 207.5 (0.917), 233.5 (0.392), and 326 nm (0.535); ECD (MeOH) λ_{max} ($\Delta\varepsilon$) 207 (−5.08), 224 (−0.63), 251 (+2.44), and 316 (−0.50); ^1H and ^{13}C NMR data in Table 3; HRESIMS *m*/*z* 195.0652 $[M + H]^+$ (calcd for $C_{10}H_{11}O_4$, 195.0652).

Computational Details

3D models of **1** and **2** were built and geometry optimized using Spartan'10. Conformational analysis was performed by a Monte Carlo search protocol as implemented in the same software under an MMFF94 molecular mechanics force field. The resulting conformers were filtered and checked for duplicity. All conformers were minimized using a DFT force field at the B3LYP/DGDZVP level of theory employing the Gaussian 09 program package. The conformers were optimized, and thermochemical properties, IR, and vibrational analyses were obtained at the same level of theory. The self-consistent reaction field with conductor-like continuum solvent model was used to perform the ECD calculations of the major conformers of **1** (**1a**–**1d**), **2** (**2a**–**2c**), and **3** in MeOH solution. The calculated excitation energy (nm) and rotatory strength (*R*) in dipole velocity (R_{vel}) and dipole length (R_{len}) forms were simulated into an ECD curve. Magnetic shielding tensors were calculated with the gauge-invariant atomic orbital method (GIAO), and coupling constants (^1H–^1H) were obtained from the B3LYP/DGDZVP-optimized structures using the spin–spin option during the NMR calculations. All calculations were performed on the NES cluster, a parallel supercomputer with a Linux operating system, containing 250 nodes with two processors at 2.6 GHz and eight cores (32 GB RAM) each.

Enzymatic Assays

The fungal extract, fractions, compounds, and acarbose (positive control) were dissolved in MeOH or phosphate buffer solution (PBS, 100 mM, pH 7). Aliquots of 0–10 µL of testing materials (triplicated) were incubated for 10 min with 20 µL of enzyme stock solution (0.4 units/mL) in PBS. After incubation, 10 µL of substrate (*p*NPG 5 mM) was added and incubated a further 20 min at 37 °C, and the absorbances were determined.(17)

For the extract and fractions, the inhibitory activity was determined as percentage in comparison to the blank (MeOH) according to the following equation: $$\%\ \alpha\text{GHY} = \left(1 - \frac{A_{405}t}{A_{405}c}\right) \times 100\%$$ where %

αGHY is the percentage of inhibition, $A_{405}t$ is the corrected absorbance of the extract, fractions, or compound under testing ($A_{405\ \text{end}} - A_{405\ \text{initial}}$), and $A_{405}c$ is the absorbance of the blank ($A_{405\ \text{end blank}} - A_{405\ \text{initial blank}}$). The IC_{50} was calculated by regression analysis, using the following equation: $$\%\ \text{Inhibition} = \frac{A_{100}}{1 + \left(\frac{I}{IC_{50}}\right)^{s}}$$ where A_{100} is the maximum inhibition, I is the inhibitor concentration, IC_{50} is the concentration required to inhibit activity of the enzyme by 50%, and s is the cooperative degree.(21)

Molecular Docking

The αGHY crystallographic structure was downloaded from the Protein Data Bank site (PDB: 3A4A; http://www.rcsb.org/pdb/). Subsequently all hydrogen and Kolleman charges were assigned to the receptor using AutoDockTools 1.5.4. The files were saved in proper format for use with Autogrid4.0 and AutoDock4.0 systems. Compounds **2** and **3** were built using the program Spartan'10 (www.wavefunction.com) and optimized geometrically using the program Gaussian 09, revision A.02 (Gaussian Inc., Wallingford, CT, USA) at the DFT B3LYP/DGDZVP level of theory. The ligands were prepared by assigning the Gasteiger–Marsili atomic charges and nonpolar hydrogens using AutoDockTools 1.5.4 (http://mgltools.scripps.edu/). Binding pockets of enzymes and docking simulation were predicted using AutoDock 4.0 (http://autodock.scripps.edu/). Initially, a blind docking was performed; then, the best energy result from the previous procedure was used as the initial conformation to undertake simulation. Docking studies were done with Lamarckian Genetic Algorithm (LGA).(18, 22, 23) The grid box for docking was set around a central atom of the ligand with dimensions of 30 × 30 × 30 Å. Parameters were set to an LGA calculation of 100 runs, whereas energy evaluations were set to 2 500 000 and 27 000 generations (repetition of process). The resulting docked poses were analyzed with AutoDockTools using cluster analysis, PyMOL.(24)

Supporting Information

Calculated DFT B3LYP/DGDZVP free energies, population, and theoretical averaged rotatory strength values expressed in $R_{(len)}$ for **1a**–**1d**. Calculated DFT B3LYP/DGDZVP free energies, population, and theoretical averaged coupling constant values for **1a** and **1b**. Calculated DFT B3LYP/DGDZVP free energies, population, and theoretical averaged rotatory strength values expressed in $R_{(len)}$ for **2a**–**2c** and **3**. ^{1}H, ^{13}C, HSQC, HMBC, COSY, and ROESY spectra of compound **1**. HRESIMS spectrum of compound **1**. Double resonance experiments (selective irradiation δ_H 2.35 and 2.67 ppm) of compound **1**. ^{1}H, ^{13}C, HSQC, HMBC, and COSY spectra of compound **2**. ^{1}H, ^{13}C, HSQC, HMBC, and COSY spectra of compound **3**. Enzymatic inhibitory activity of compounds **2** and **3** against *Saccharomyces cerevisiae* α-glucosidase (αGHY; A and B, respectively). This material is available free of charge via the Internet at http://pubs.acs.org.

Acknowledgment

This work was supported by a grant from CONACyT (219765). We thank I. Rivero, A. Pérez, and S. Cristians for their valuable assistance. J.R.-C. acknowledges a fellowship from CONACyT to pursue graduate studies. We are indebted to Dirección General de Cómputo y de

Tecnologías de Información y Comunicación (DGTIC), UNAM, for providing the resources to carry out computational calculations through the Miztli System.

References

1. Ainsworth, G. C. Ainsworth & Bisby's Dictionary of the Fungi; CABI, **2008**.
2. Song, F.; Wu, S.-H.; Zhai, Y.-Z.; Xuan, Q.-C.; Wang, T. Chem. Biodiversity **2014**, 11, 673– 694
3. Baraban, E. G.; Morin, J. B.; Phillips, G. M.; Phillips, A. J.; Strobel, S. A.; Handelsman, J. Tetrahedron Lett. **2013**, 54 (31) 4058– 4060
4. Aguiree, F.; Brown, A.; Cho, N. H.; Dahlquist, G.; Dodd, S. IDF Diabetes Atlas, 6th ed.; International Diabetes Federation, **2013**; pp 11– 49.
5. Israili, Z. H. Am. J. Ther. **2011**, 18, 117– 152
6. Mata, R.; Cristians, S.; Escandón-Rivera, S.; Juárez-Reyes, K.; Rivero-Cruz, I. J. Nat. Prod. **2013**, 76, 468– 483
7. Devys, M.; Barbier, M.; Bousquet, J. F.; Kollmann, A. Z. Naturforsch. **1992**, 779– 781
8. Tansuwan, S.; Pornpakakul, S.; Roengsumran, S.; Petsom, A.; Muangsin, N.; Sihanonta, P.; Chaichit, N. J. Nat. Prod. **2007**, 70, 1620– 1623
9. Tansuwan, S.; Chanaprat, P.; Teerawatananond, T.; Muangsin, N.; Pornpakakul, S. Acta Crystallogr. **2010**, E66 (2263) 1– 8
10. He, J.; Wijeratne, E. M. K.; Bashyal, B. P.; Zhan, J.; Seliga, C. J.; Liu, M. X.; Pierson, E. E.; Pierson, L. S.; VanEtten, H. D.; Gunatilaka, A. A. L. J. Nat. Prod. **2004**, 67, 1985– 1991
11. Kimura, Y.; Tamura, S. Agric. Biol. Chem. **1972**, 36, 1925– 1930
12. Akay, Ş.; Ekiz, G.; Kocabaş, F.; Hameş-Kocabaş, E. E.; Korkmaz, K. S.; Bedir, E. Phytochem. Lett. **2014**, 7, 93– 96
13. Acuña, U. M.; Figueroa, M.; Kavalier, A.; Jancovski, N.; Basile, M. J.; Kennelly, E. J. J. Nat. Prod. **2010**, 73, 1775– 1779
14. (a) Mendoza-Espinoza, J. A.; López-Vallejo, F.; Fragoso-Serrano, M.; Pereda-Miranda, R.; Cerda-García-Rojas, C. M. J. Nat. Prod. **2009**, 72, 700– 708

    (b) López-Vallejo, F.; Suárez-Ortiz, G. A.; Hernández-Rojas, A. C.; Cerda García-Rojas, C. M.; Pereda-Miranda, R. J. Org. Chem. **2011**, 76, 6057– 6066
15. Krohn, K.; Bahramsari, R.; Flörke, U.; Ludewig, K.; Kliche-Spory, C.; Michel, A.; Aust, H. J.; Draeger, S.; Schulz, B.; Antus, S. Phytochemistry **1997**, 45, 313– 320
16. Oki, T.; Matsui, T.; Osajima, Y. J. Agric. Food Chem. **1999**, 47, 550– 553
17. Rivera-Chávez, J.; González-Andrade, M.; González, M. D. C.; Glenn, A. E.; Mata, R. Phytochemistry **2013**, 94, 198– 205

18. Morris, G. M.; Goodsell, D. S.; Halliday, R. S.; Huey, R.; Hart, W. E.; Belew, R. K.; Olson, A. J. J. Comput. Chem. **1998**, 19, 1639– 1662

19. Rudnitskaya, A.; Török, B.; Török, M. Biochem. Mol. Biol. Educ. **2010**, 38, 261– 265

20. Rodriguez, R. J.; White, J. F., Jr.; Arnold, A. E.; Redman, R. S. New Phytol. **2009**, 182, 314– 330

21. Copeland, R. A. Enzymes: A Practical Introduction to Structure, Mechanism, and Data Analysis, 2nd ed.; Wiley-VCH, **2000**.

22. Rudnitskaya, A.; Török, B.; Török, M. Biochem. Mol. Biol. Educ. **2010**, 38, 261– 265

23. Çifci, G.; Aviyente, V.; Akten, E. D. Mol. Inf. **2012**, 31, 459– 471

24. PyMOL; DeLano Scientific **, 2002**

α-Glucosidase Inhibitors from a *Xylaria feejeensis* Associated with *Hintonia latiflora*

José Rivera-Chávez,[†,‡] *Mario Figueroa,*[†] *María del Carmen González,*[§] *Anthony E. Glenn,*[⊥] *and Rachel Mata**[,†]

[†]Facultad de Química, Universidad Nacional Autónoma de México, México DF 04510, Mexico.

[§]Instituto de Biología, Universidad Nacional Autónoma de México, México DF 04510, Mexico.

[⊥]Toxicology & Mycotoxin Research Unit, 950 College Station Road, USDA ARS Russell Research Center, Athens, GA 30605, USA.

List of contents

Figure S23. Distance phylogram based on blastn of the ITS region. The *H. latiflora* endophyte is the query (yellow highlight)

Tabla S1. Energía libre de Gibbs calculada (DFT B3LYP/DGDZVP), población y valores de fuerza de rotación teóricos expresados en $R_{(vel)}$ para los confórmeros más relevantes del diastereoisómero **1a**

conformer	ΔG^a	$P(\%)^b$	*n* states[c]														
			1	2	3	4	5	6	7	8	9	10	11	12	13	14	15
1	0.000	0.485	8.15	0.08	-48.11	2.77	-9.81	36.66	1.98	-0.69	-0.41	-1.43	-2.40	-0.64	4.07	-7.75	-1.13
2	0.339	0.274	-0.04	0.01	-27.93	3.77	9.80	13.19	0.52	-0.36	-0.23	6.14	-0.27	0.48	-6.31	-8.62	-32.41
3	0.564	0.187	8.07	0.02	-52.49	4.32	5.95	21.05	4.03	-0.63	-0.49	-0.78	-2.32	-1.64	1.60	-6.18	-1.10
4	1.668	0.029	8.55	0.03	-54.58	3.94	8.03	21.06	2.59	-0.51	-0.30	0.45	-1.68	-1.26	-8.12	-0.24	-4.19
5	1.769	0.024	9.75	0.05	-52.46	-1.00	-6.58	38.93	-1.06	-0.24	-0.23	-1.50	-3.28	2.29	-1.60	-6.21	-4.34
Weighted value[d]			16.73	0.09	-114.3	6.70	3.59	63.53	3.91	-1.18	-0.80	1.39	-4.83	-0.37	-5.03	-14.07	-20.95
Averaged λ (nm)[e]			331.8	279.5	259.0	243.8	237.9	233.4	228.4	219.4	207.5	198.3	194.7	191.4	189.1	188.0	185.6

[a]DFT B3LYP/DGDZVP Gibbs free energies in kcal mol-1 relative to the absolute G value for the global minimum -870120.1837 kcal mol^{-1}. [b]In percent from ΔG values at 298 K and 1 atm. [c]DFT B3LYP/DGDZVP Rotatory strength values expressed in $R_{(vel)}$. [d]Calculated with the equation $\Sigma^i R_{(vel)}{}^i \times P^i$, where $R_{(vel)}{}^i$ is the theoretical $R_{(vel)}$ value calculated for the $n = 1 \rightarrow 15$ excitation state and P^i is the population for the i^{th} conformer. [e]Averaged excitation state.

Table S2. Calculated DFT B3LYP/DGDZVP Free Energies, Population and Theoretical Averaged Rotatory Strength Values Expressed in $R_{(vel)}$ for the Most Relevant Conformations of Diastereoisomer**1b**

conformer	ΔG^a	$P(\%)^b$	*n* states[c]													
			1	2	3	4	5	6	7	8	9	10	11	12	13	14	15
1	0.000	0.710	4.58	-0.22	66.45	-31.38	0.24	-0.37	-7.67	-16.22	0.51	-3.69	17.15	0.73	0.41	0.99	-8.93
2	0.530	0.290	4.21	-0.12	-39.27	-0.59	21.32	16.06	-0.44	0.12	-1.39	-1.64	0.94	-8.69	-9.41	-8.64	-1.45
Weighted value[d]			4.47	-0.19	35.77	-22.44	6.36	4.40	-5.57	-11.47	-0.04	-3.10	12.45	-2.01	-2.44	-1.80	-6.76
Averaged λ (nm)[e]			330.0	279.9	259.4	245.5	242.6	237.2	225.2	217.7	207.4	204.0	197.1	193.0	190.3	188.6	187.6

[a]DFT B3LYP/DGDZVP Gibbs free energies in kcal mol-1 relative to the absolute G value for the global minimum -870119.8268 kcal mol^{-1}. [b]In percent from ΔG values at 298 K and 1 atm. [c]DFT B3LYP/DGDZVP Rotatory strength values expressed in $R_{(vel)}$. [d]Calculated with the equation $\Sigma^i R_{(vel)}{}^i \times P^i$, where $R_{(vel)}{}^i$ is the theoretical $R_{(vel)}$ value calculated for the $n = 1 \rightarrow 15$ excitation state and P^i is the population for the i^{th} conformer. [e]Averaged excitation state.

Table S3. Calculated DFT B3LYP/DGDZVP Free Energies, Population and Theoretical Averaged Rotatory Strength Values Expressed in $R_{(vel)}$ for the Most Relevant Conformations of Diastereoisomer **1c**

conformer	ΔG^a	$P(\%)^b$	*n* states[c]													
			1	2	3	4	5	6	7	8	9	10	11	12	13	14	15
1	0.000	0.536	-2.17	0.18	32.46	-4.98	8.79	-31.02	1.00	-0.14	0.12	-0.19	-0.65	1.37	-3.82	8.47	36.08
2	0.358	0.293	-3.26	0.11	29.64	-0.64	-18.36	-11.23	1.86	0.23	0.34	6.19	-3.05	6.12	0.47	0.54	26.52
3	1.197	0.071	-3.16	0.12	29.11	-1.59	-18.13	-10.40	1.96	0.23	0.30	8.48	-3.91	-1.62	4.48	2.46	23.38
4	1.252	0.065	-3.22	0.10	30.55	-0.46	-28.77	-2.53	2.64	0.16	0.61	7.67	-4.45	2.01	6.39	0.07	14.62
5	1.621	0.035	-1.65	0.32	28.69	-5.59	-22.57	-10.77	5.20	0.79	1.02	-1.77	12.68	18.89	6.18	2.79	-17.88
Weighted value[d]			-2.61	0.16	31.14	-3.19	-4.60	-21.20	1.57	0.05	0.26	2.75	-1.37	3.20	-0.96	4.97	29.11
Averaged λ (nm)[e]			329.2	275.7	258.7	239.5	235.4	232.7	227.9	217.1	205.3	198.7	193.9	190.4	187.9	186.7	184.6

[a]DFT B3LYP/DGDZVP Gibbs free energies in kcal mol-1 relative to the absolute G value for the global minimum -870120.7017 kcal mol^{-1}. [b]In percent from ΔG values at 298 K and 1 atm. [c]DFT B3LYP/DGDZVP Rotatory strength values expressed in $R_{(vel)}$. [d]Calculated with the equation $\Sigma^i R_{(vel)}{}^i \times P^i$, where $R_{(vel)}{}^i$ is the theoretical $R_{(vel)}$ value calculated for the $n = 1 \rightarrow 15$ excitation state and P^i is the population for the i^{th} conformer. [e]Averaged excitation state.

Table S4. Calculated DFT B3LYP/DGDZVP Free Energies, Population and Theoretical Averaged Rotatory Strength Values Expressed in $R_{(vel)}$ for the Most Relevant Conformations of Diastereoisomer **1d**

conformer	ΔG^a	$P(\%)^b$	*n* states[c]													
			1	2	3	4	5	6	7	8	9	10	11	12	13	14	15
1	0.000	0.547	-4.94	0.19	39.40	-6.68	-30.24	4.86	1.72	-0.47	-0.03	-1.52	8.60	6.32	0.76	2.56	4.34
2	0.451	0.257	-1.44	0.31	32.93	-4.03	-0.34	-23.90	-2.78	1.34	0.54	-7.51	3.18	7.92	3.60	-0.45	32.01
3	0.766	0.151	-0.78	-0.06	32.99	-8.62	-23.56	-0.95	1.77	-0.91	-1.01	-2.22	2.06	4.88	8.53	-1.21	20.37
4	1.517	0.042	-0.72	-0.07	30.46	-8.00	-23.66	-1.13	2.35	-0.96	-1.11	-2.19	1.22	2.01	8.08	2.90	15.13
Weighted value[d]			-3.22	0.17	36.27	-6.33	-21.18	-3.67	0.59	-0.09	-0.08	-3.19	5.88	6.31	2.97	1.23	14.31
Averaged λ (nm)[e]			328.4	274.3	258.3	240.2	235.0	233.3	226.9	215.1	204.6	198.5	193.7	190.2	187.4	185.9	184.6

[a]DFT B3LYP/DGDZVP Gibbs free energies in kcal mol-1 relative to the absolute G value for the global minimum -870120.7017 kcal mol^{-1}. [b]In percent from ΔG values at 298 K and 1 atm. [c]DFT B3LYP/DGDZVP Rotatory strength values expressed in $R_{(vel)}$. [d]Calculated with the equation $\Sigma^i R_{(vel)}{}^i \times P^i$, where $R_{(vel)}{}^i$ is the theoretical $R_{(vel)}$ value calculated for the $n = 1 \rightarrow 15$ excitation state and P^i is the population for the i^{th} conformer. [e]Averaged excitation state.

Table S5. Calculated DFT B3LYP/DGDZVP Free Energies, Population and Theoretical Averaged ^3J Values for the Most Relevant Conformations of Diastereoisomer **1a**

conformer	ΔG^a	$P(\%)^b$	$^3J_{6\text{-}7}{}^c$	$^3J_{5proR\text{-}6}{}^c$	$^3J_{5proS\text{-}6}{}^c$
1	0.000	0.485	8.09	3.62	12.96
2	0.339	0.274	4.23	3.42	13.13
3	0.564	0.187	8.65	3.45	12.96
4	1.668	0.029	8.6	3.49	12.96
5	1.769	0.024	8.18	3.68	12.91
Weighted value[d]			7.16	3.53	13.01

[a]DFT B3LYP/DGDZVP Gibbs free energies in kcal mol-1 relative to the absolute G value for the global minimum -870120.7017 kcal mol^{-1}. [b]In percent from ΔG values at 298 K and 1 atm. [c]DFT B3LYP/DGDZVP $^3\boldsymbol{J}$ values expressed in Hz. [d]Calculated with the equation $\Sigma^i \boldsymbol{J}^i \times P^i$, where $\boldsymbol{J}^i$ is the theoretical coupling constant value (spin-spin constant) and P^i is the population for the i^{th} conformer.

Table S6. Calculated DFT B3LYP/DGDZVP Free Energies, Population and Theoretical Averaged ^3J Values for the Most Relevant Conformations of Diastereoisomer **1b**

conformer	ΔG^a	$P(\%)^b$	$^3J_{6\text{-}7}{}^c$	$^3J_{5proR\text{-}6}{}^c$	$^3J_{5proS\text{-}6}{}^c$
1	0.000	0.710	9.64	6.94	0.97
2	0.530	0.290	3.02	3.4	12.35
Weighted value[d]			7.72	5.91	4.27

[a]DFT B3LYP/DGDZVP Gibbs free energies in kcal mol-1 relative to the absolute G value for the global minimum -870119.8268 kcal mol^{-1}. [b]In percent from ΔG values at 298 K and 1 atm. [c]DFT B3LYP/DGDZVP ^3J values expressed in Hz. [d]Calculated with the equation $\Sigma^i J^i \times P^i$, where J^i is the theoretical coupling constant value (spin-spin constant) and P^i is the population for the i^{th} conformer.

Table S7. DFT Calculated and Experimental $^{1}H–^{1}H$ Coupling Constants of **1**

$^{3}J_{H\text{-}H}$	experimental	calculated coupling constants[a]	
		1a	**1b**
$J_{6,7}$	5.5	6.5[b]	7.0[b]
$J_{5proR,\,6}$	3.8	3.5	5.9
$J_{5proS,\,6}$	12.6	13.0	4.3
rmsd	-	0.64	5.03

Coupling constants are expressed in Hz. [a]Theoretical coupling constants were calculated at B3LYP/DGTZVP level of theory. Coupling constants were Boltzman-weighted using the $\Sigma_i J^i \times P^i$, where J^i is the coupling constant value for each conformer and P^i is the population of the conformation. [b]The averaged coupling constants were scaled with the factor: $f_{H(sp3)\text{-}H(sp3)} = 0.910$.

Table S8. Calculated DFT B3LYP/DGDZVP Free Energies, Population and Theoretical Averaged Rotatory Strength Values Expressed in $R_{(vel)}$ for the Most Relevant Conformations of Diastereoisomer **2a**

conformer	ΔG^a	$P(\%)^b$	*n* states[c]													
			1	2	3	4	5	6	7	8	9	10	11	12	13	14	15
1	0.000	0.383	7.12	9.60	-11.06	-13.37	-5.71	37.69	21.87	-24.17	-29.75	-2.87	-30.89	30.90	16.36	11.80	7.12
2	0.116	0.314	7.10	9.60	-11.08	-13.37	-5.73	37.74	21.83	-24.02	-29.86	-2.89	-30.80	30.79	16.42	11.79	7.10
3	0.444	0.181	7.11	9.60	-11.06	-13.39	-5.74	37.73	21.81	-23.86	-29.99	-2.84	-30.79	30.82	16.40	11.80	7.11
4	0.924	0.080	7.12	9.55	-10.97	-13.44	-5.73	37.68	21.80	-23.84	-29.98	-2.78	-30.83	30.85	16.43	11.78	7.12
5	1.505	0.030	7.09	9.60	-11.13	-13.34	-5.76	37.80	21.76	-23.76	-30.12	-2.85	-30.71	30.77	16.43	11.80	7.09
6	2.132	0.010	7.13	9.55	-11.25	-13.18	-5.70	37.79	21.79	-24.01	-29.97	-2.83	-30.82	30.98	16.40	11.76	7.13
Weighted value[d]			7.11	9.60	-11.06	-13.38	-5.73	37.71	21.83	-24.03	-29.86	-2.87	-30.84	30.85	16.39	11.79	16.50
Averaged λ (nm)[e]			359.4	270.4	257.7	252.9	230.1	213.4	207.4	196.2	194.2	192.4	189.1	184.4	183.2	174.9	171.3

[a]DFT B3LYP/DGDZVP Gibbs free energies in kcal mol-1 relative to the absolute G value for the global minimum -431786.0152 kcal mol^{-1}. [b]In percent from ΔG values at 298 K and 1 atm. [c]DFT B3LYP/DGDZVP Rotatory strength values expressed in $R_{(vel)}$. [d]Calculated with the equation $\Sigma^i R_{(vel)}{}^i \times P^i$, where $R_{(vel)}{}^i$ is the theoretical $R_{(vel)}$value calculated for the $n = 1 \rightarrow 15$ excitation state and P^i is the population for the i^{th} conformer. [e]Averaged excitation state.

Table S9. Calculated DFT B3LYP/DGDZVP Free Energies, Population and Theoretical Averaged Rotatory Strength Values Expressed in $R_{(vel)}$ for the Most Relevant Conformations of Diastereoisomer **2b**

conformer	ΔG^a	$P(\%)^b$	*n* states[c]														
			1	2	3	4	5	6	7	8	9	10	11	12	13	14	15
1	0.000	0.325	-0.61	7.55	21.80	-33.95	-29.63	-3.10	23.91	13.52	32.94	-9.31	32.77	-28.01	-30.34	29.31	6.05
2	0.074	0.287	-0.60	7.59	21.82	-33.99	-29.69	-3.08	23.99	13.53	33.05	-9.33	32.75	-28.12	-30.27	29.25	6.03
3	0.286	0.201	-0.61	7.59	21.83	-34.00	-29.71	-3.06	24.01	13.54	33.07	-9.36	32.75	-28.16	-30.25	29.23	6.02
4	0.619	0.115	-0.62	7.60	21.85	-34.01	-29.72	-3.04	24.02	13.53	33.10	-9.40	32.74	-28.19	-30.22	29.22	6.02
5	1.046	0.056	-0.60	7.61	21.84	-34.04	-29.74	-3.04	24.01	13.55	33.19	-9.40	32.69	-28.23	-30.18	29.21	6.01
6	1.776	0.016	-0.60	7.61	21.83	-34.03	-29.73	-3.04	24.00	13.55	33.21	-9.39	32.67	-28.21	-30.18	29.23	6.01
Weighted value[d]			-0.61	7.58	21.82	-33.99	-29.68	-3.08	23.97	13.53	33.04	-9.34	32.75	-28.11	-30.28	29.26	6.03
Averaged λ (nm)[e]			357.0	277.5	263.2	241.7	230.6	208.3	205.4	199.7	194.3	189.6	186.0	182.5	180.0	171.9	170.4

[a]DFT B3LYP/DGDZVP Gibbs free energies in kcal mol-1 relative to the absolute G value for the global minimum -431786.4058 kcal mol^{-1}. [b]In percent from ΔG values at 298 K and 1 atm. [c]DFT B3LYP/DGDZVP Rotatory strength values expressed in $R_{(vel)}$. [d]Calculated with the equation $\Sigma^i R_{(vel)}{}^i \times P^i$, where $R_{(vel)}{}^i$ is the theoretical $R_{(vel)}$value calculated for the $n = 1 \rightarrow 15$ excitation state and P^i is the population for the i^{th} conformer. [e]Averaged excitation state.

Table S10. Calculated DFT B3LYP/DGDZVP Free Energies, Population and Theoretical Averaged Rotatory Strength Values Expressed in $R_{(vel)}$ for the Most Relevant Conformations of Diastereoisomer **2c**

conformer	ΔG^a	$P(\%)^b$	*n* states[c]														
			1	2	3	4	5	6	7	8	9	10	11	12	13	14	15
1	0.000	0.424	1.75	-5.77	-23.32	35.39	30.29	3.33	-24.50	-14.74	-31.41	10.14	-35.44	29.06	27.87	-31.23	-6.45
2	0.015	0.413	1.75	-2.93	-33.03	42.21	44.14	-52.28	-4.06	-0.77	-22.84	20.98	-27.98	10.32	18.18	-10.05	-18.50
3	0.951	0.085	7.78	4.91	-64.92	26.42	5.04	30.48	-12.91	22.83	-23.23	0.04	10.99	-10.30	7.62	7.34	14.25
4	1.007	0.078	9.42	-1.00	13.52	-20.13	-3.07	5.82	4.52	7.45	1.50	15.26	-32.33	-10.47	10.82	-7.48	12.46
Weighted value[d]			2.86	-3.32	-28.02	33.14	31.28	-17.15	-12.81	-4.05	-24.62	14.16	-28.16	14.90	20.82	-17.35	-8.20
Averaged λ (nm)[e]			356.1	272.7	261.6	246.2	227.0	212.6	206.4	199.6	194.6	190.6	187.3	184.5	181.2	173.4	170.4

[a]DFT B3LYP/DGDZVP Gibbs free energies in kcal mol-1 relative to the absolute G value for the global minimum -431611.2223 kcal mol^{-1}. [b]In percent from ΔG values at 298 K and 1 atm. [c]DFT B3LYP/DGDZVP Rotatory strength values expressed in $R_{(vel)}$. [d]Calculated with the equation $\Sigma^i R_{(vel)}{}^i \times P^i$, where $R_{(vel)}{}^i$ is the theoretical $R_{(vel)}$value calculated for the $n = 1 \rightarrow 15$ excitation state and P^i is the population for the i^{th} conformer. [e]Averaged excitation state.

Table S11. Calculated DFT B3LYP/DGDZVP Free Energies, Population and Theoretical Averaged Rotatory Strength Values Expressed in $R_{(vel)}$ for the Most Relevant Conformations of Diastereoisomer **3**

conformer	ΔG^a	$P(\%)^b$	*n* states[c]														
			1	2	3	4	5	6	7	8	9	10	11	12	13	14	15
1	0.000	0.791	-5.92	-10.10	10.93	13.95	4.83	-38.42	-22.95	23.83	31.86	1.98	30.97	-31.86	-16.41	-11.88	-17.43
2	0.787	0.209	-6.88	0.82	-20.99	18.07	-8.04	7.99	-0.20	1.70	-3.57	-11.56	52.08	7.16	-30.21	3.89	-19.27
Weighted value[d]			-6.12	-7.81	4.24	14.82	2.14	-28.70	-18.18	19.20	24.44	-0.86	35.39	-23.69	-19.30	-8.58	-17.82
Averaged λ (nm)[e]			357.9	272.8	260.5	248.2	228.4	213.2	207.6	195.3	194.0	191.2	187.6	184.6	181.5	173.5	171.2

[a]DFT B3LYP/DGDZVP Gibbs free energies in kcal mol-1 relative to the absolute G value for the global minimum -431687.0787 kcal mol^{-1}. [b]In percent from ΔG values at 298 K and 1 atm. [c]DFT B3LYP/DGDZVP Rotatory strength values expressed in $R_{(vel)}$. [d]Calculated with the equation $\Sigma^i R_{(vel)}{}^i \times P^i$, where $R_{(vel)}{}^i$ is the theoretical $R_{(vel)}$value calculated for the $n = 1 \rightarrow 15$ excitation state and P^i is the population for the i^{th} conformer. [e]Averaged excitation state.

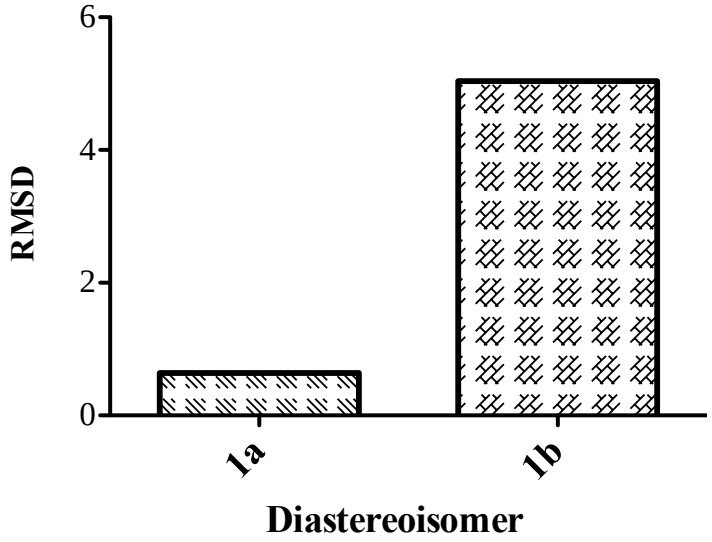

Figure S1. Comparison between experimental and theoretical $^{1}H–^{1}H$ coupling constants for **1a** and **1b** using rsmd statistics

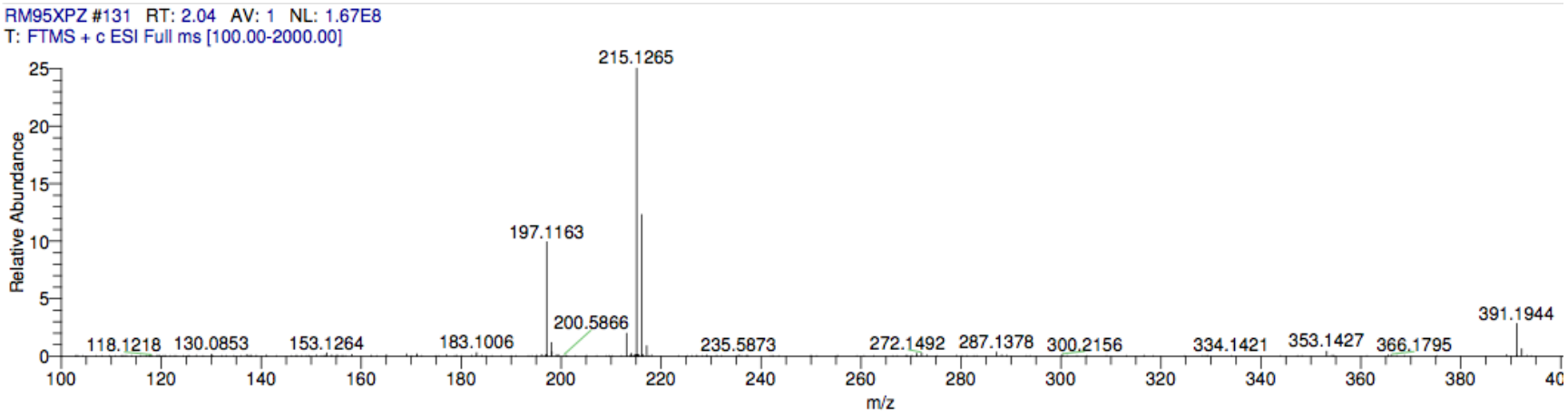

Figure S2. HRESIMS spectrum of compound **1**.

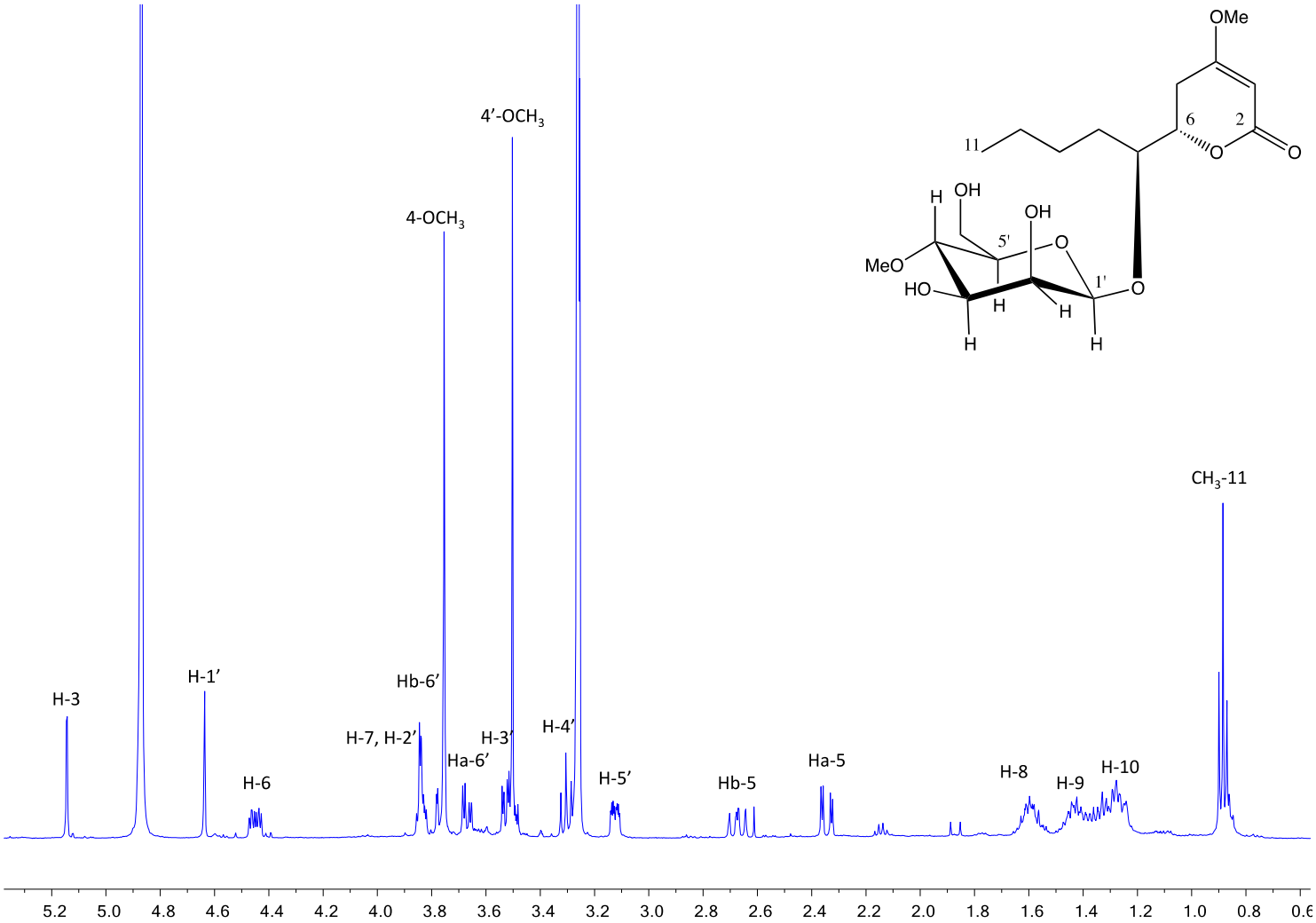

Figure S3. ^{1}H-NMR spectrum of compound **1** (500 MHz, CD_3OD).

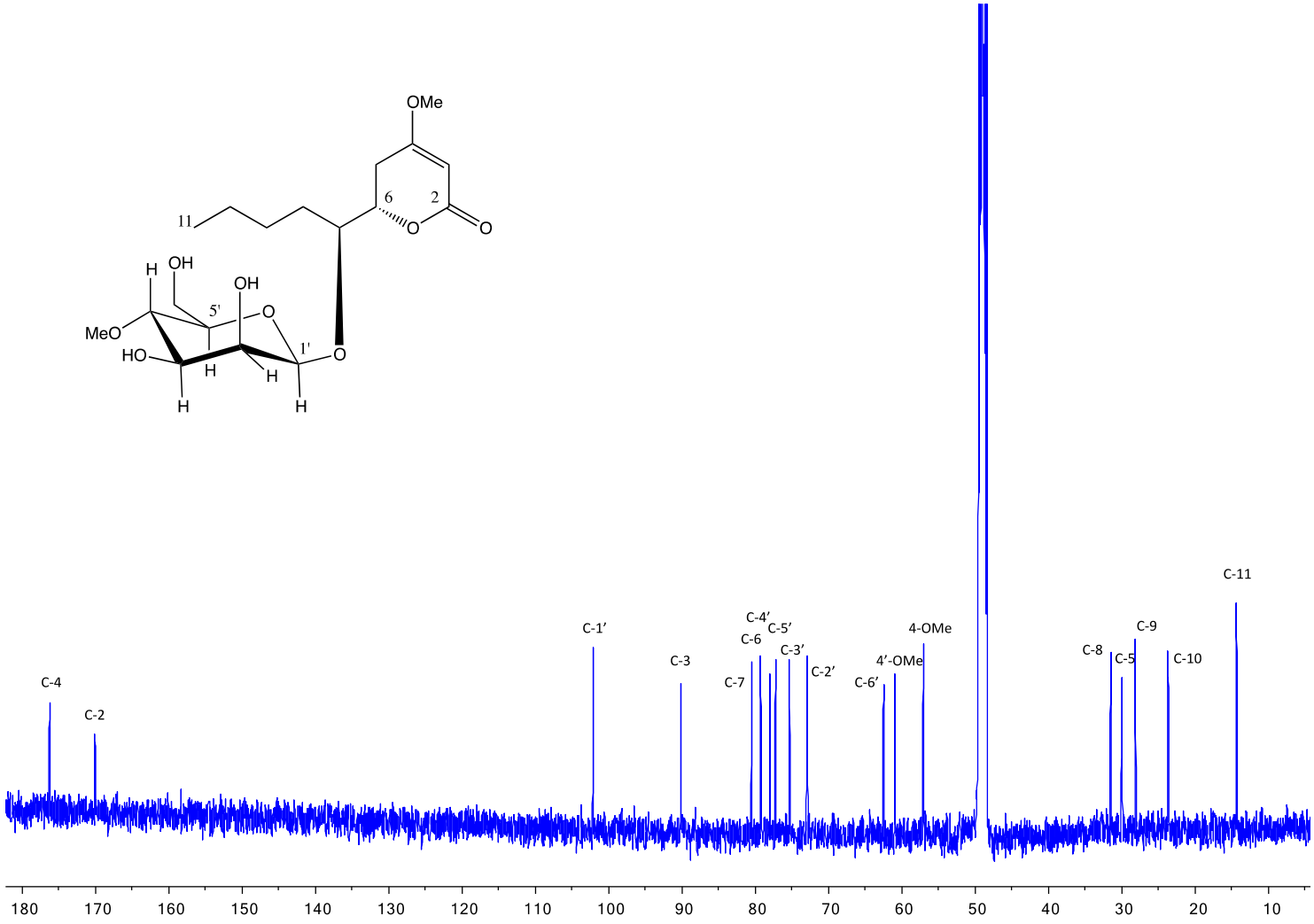

Figure S4. ^{13}C-NMR spectrum of compound **1** (125 MHz, CD_3OD).

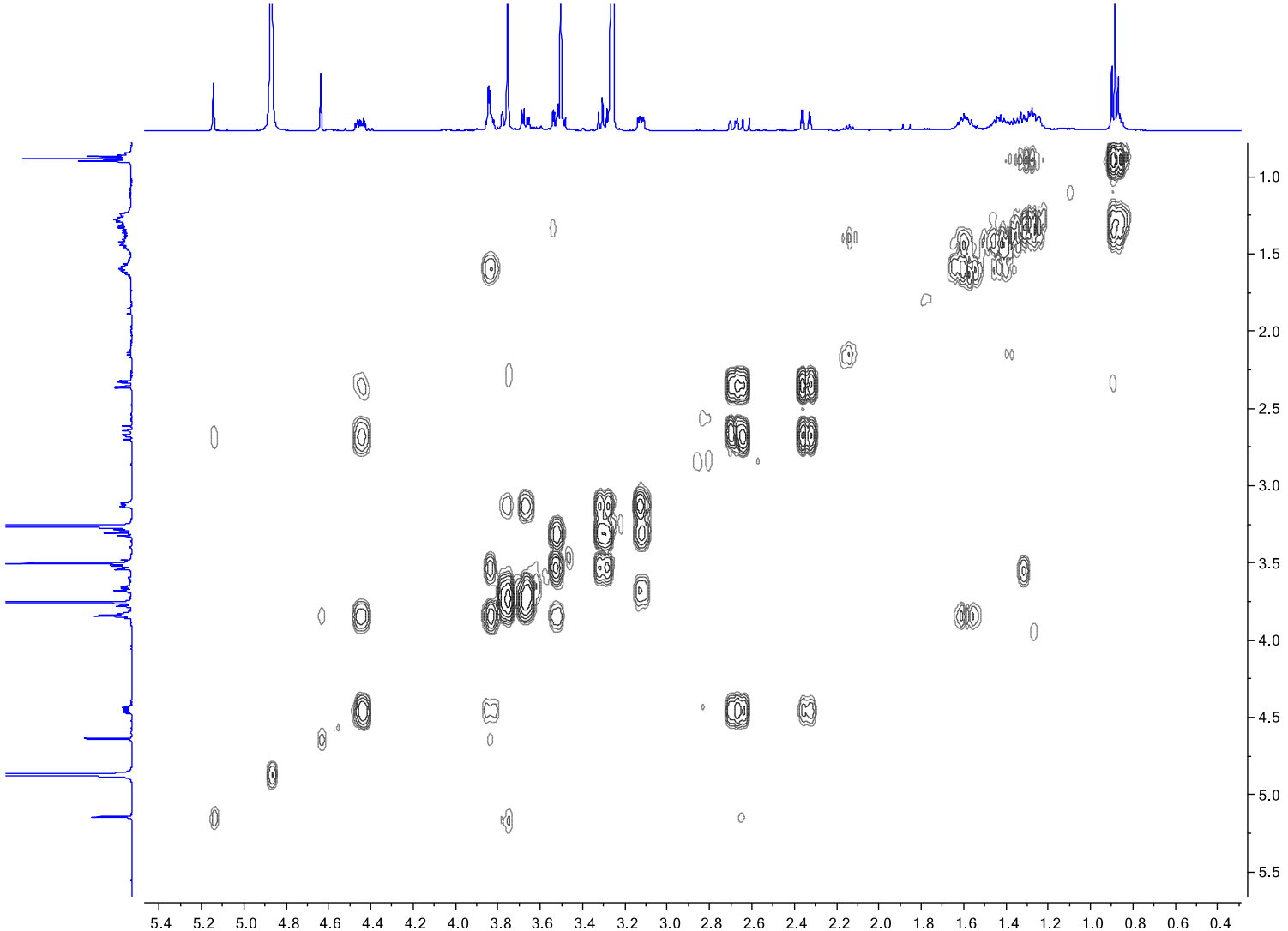

Figure S5. COSY spectrum of compound **1** (CD_3OD).

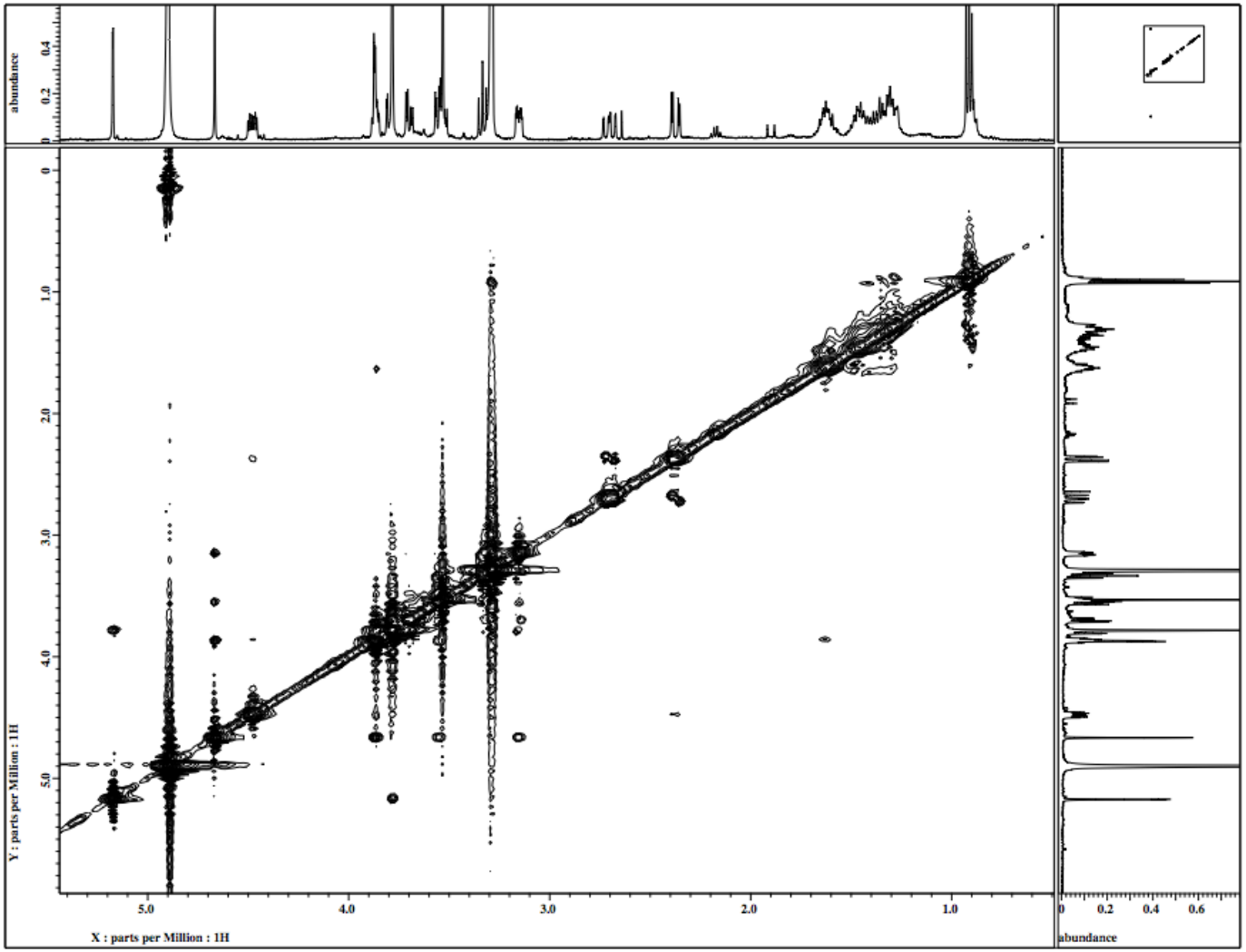

Figure S6. ROESY spectrum of compound **1** (CD_3OD).

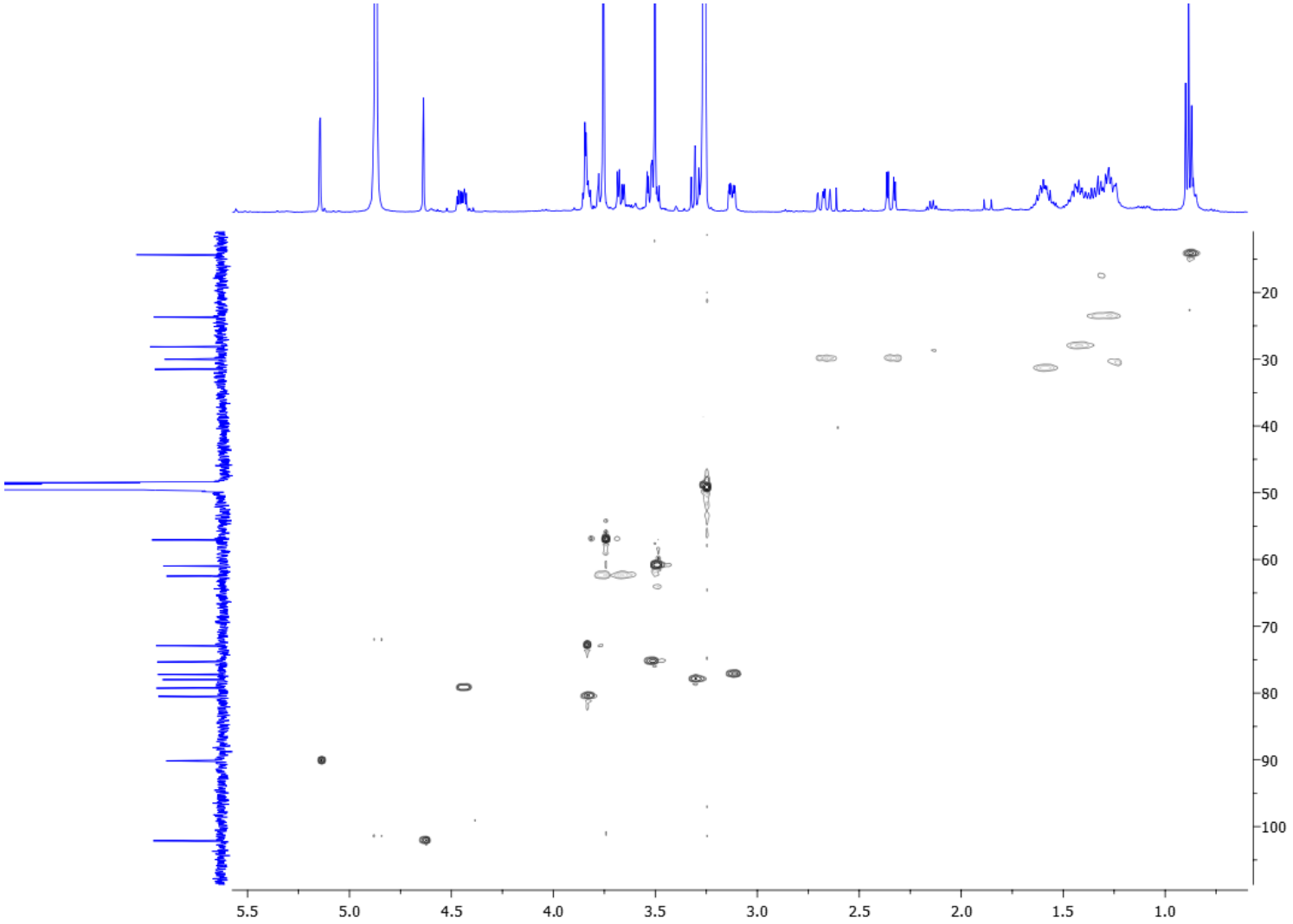

Figure S7. HSQC spectrum of compound **1** (CD_3OD).

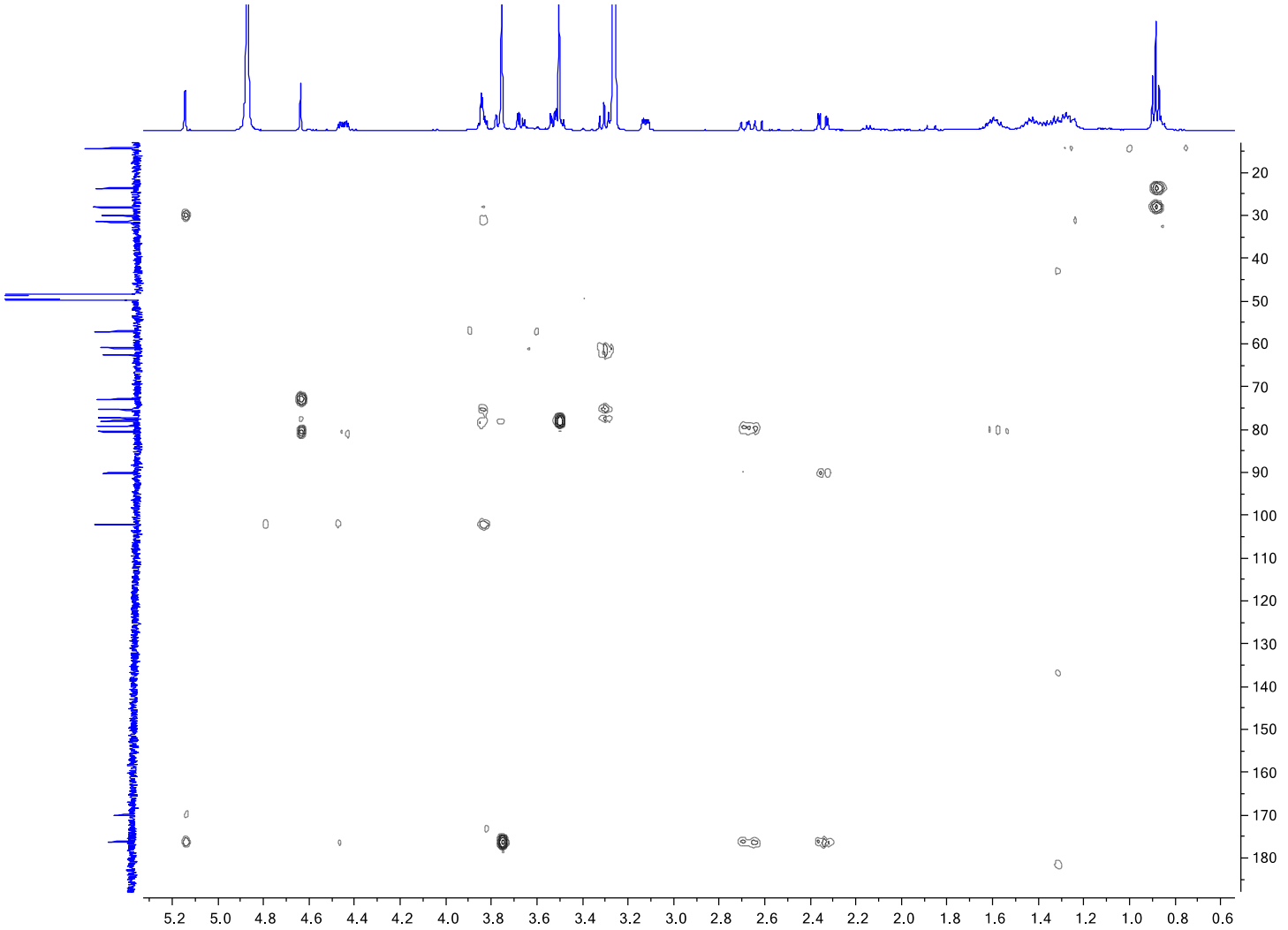

Figure S8. HMBC spectrum of compound **1** (CD_3OD).

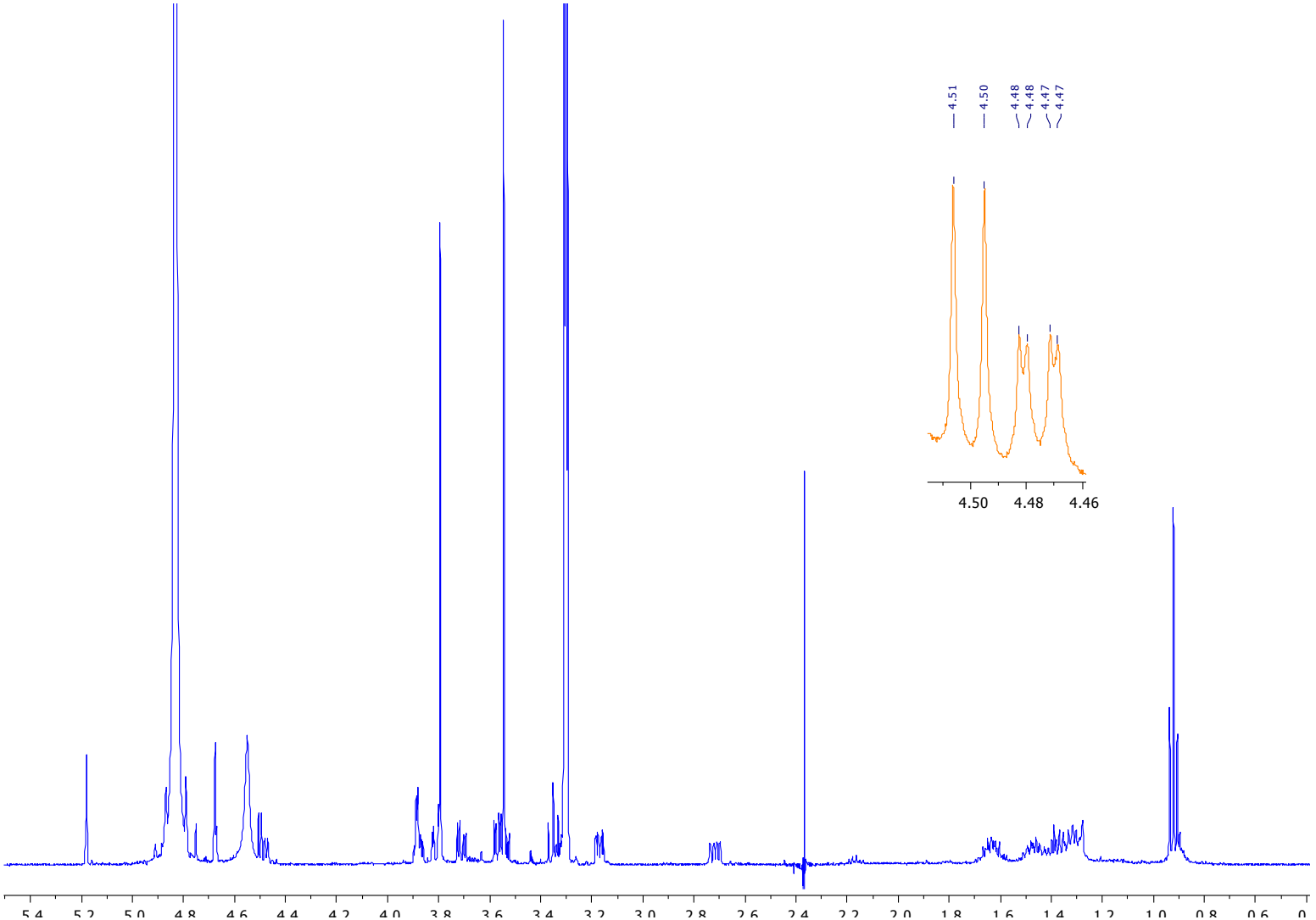

Figure S9. NOE experiment of compound **1** (CD_3OD), irradiation at 2.34 ppm.

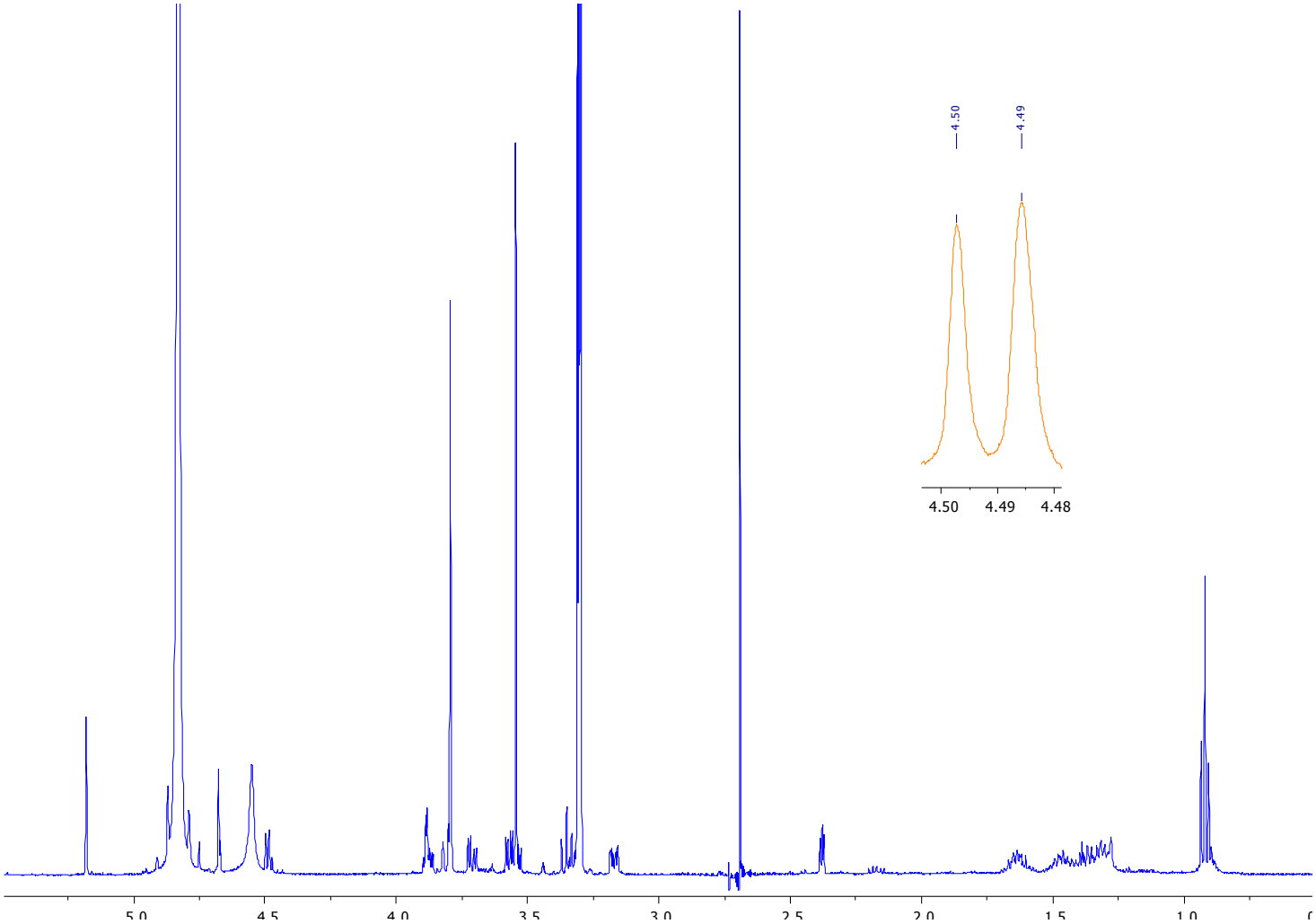

Figure S10. NOE experiment of compound **1** (CD_3OD), irradiation at 2.67 ppm.

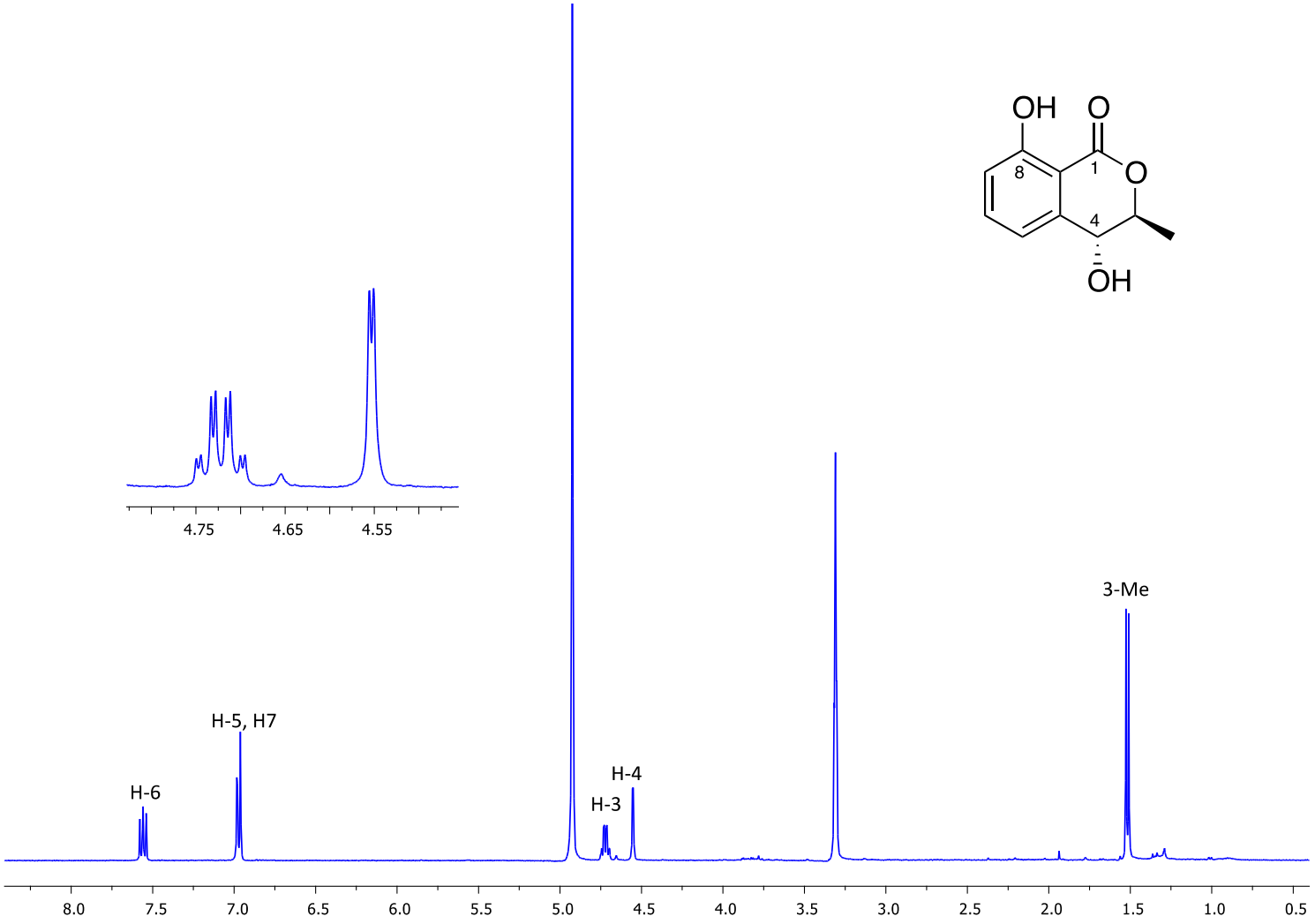

Figure S11. ^{1}H-NMR spectrum of compound **2** (400 MHz, CD_3OD).

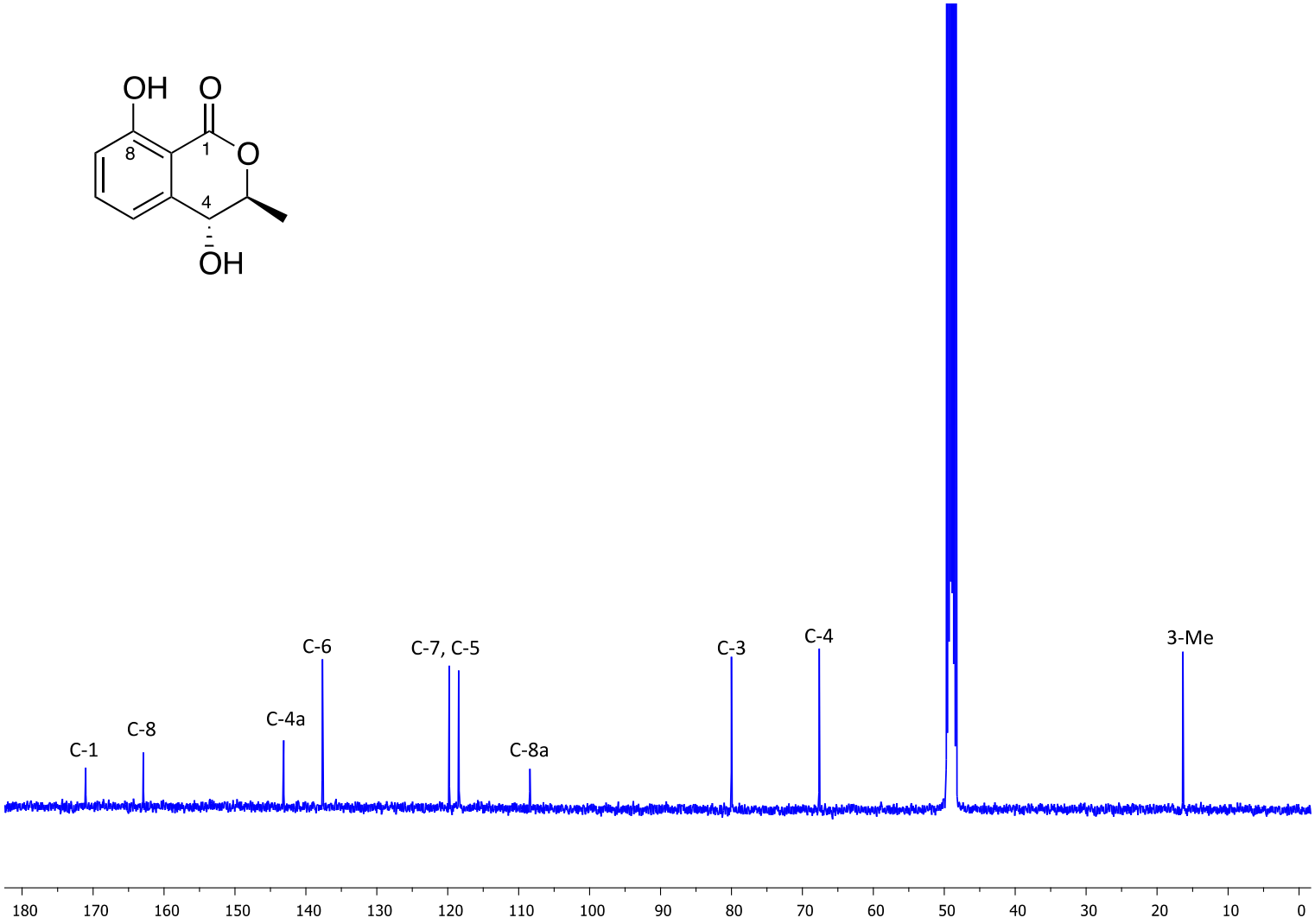

Figure S12. ^{13}C-NMR spectrum of compound **2** (100 MHz, CD_3OD).

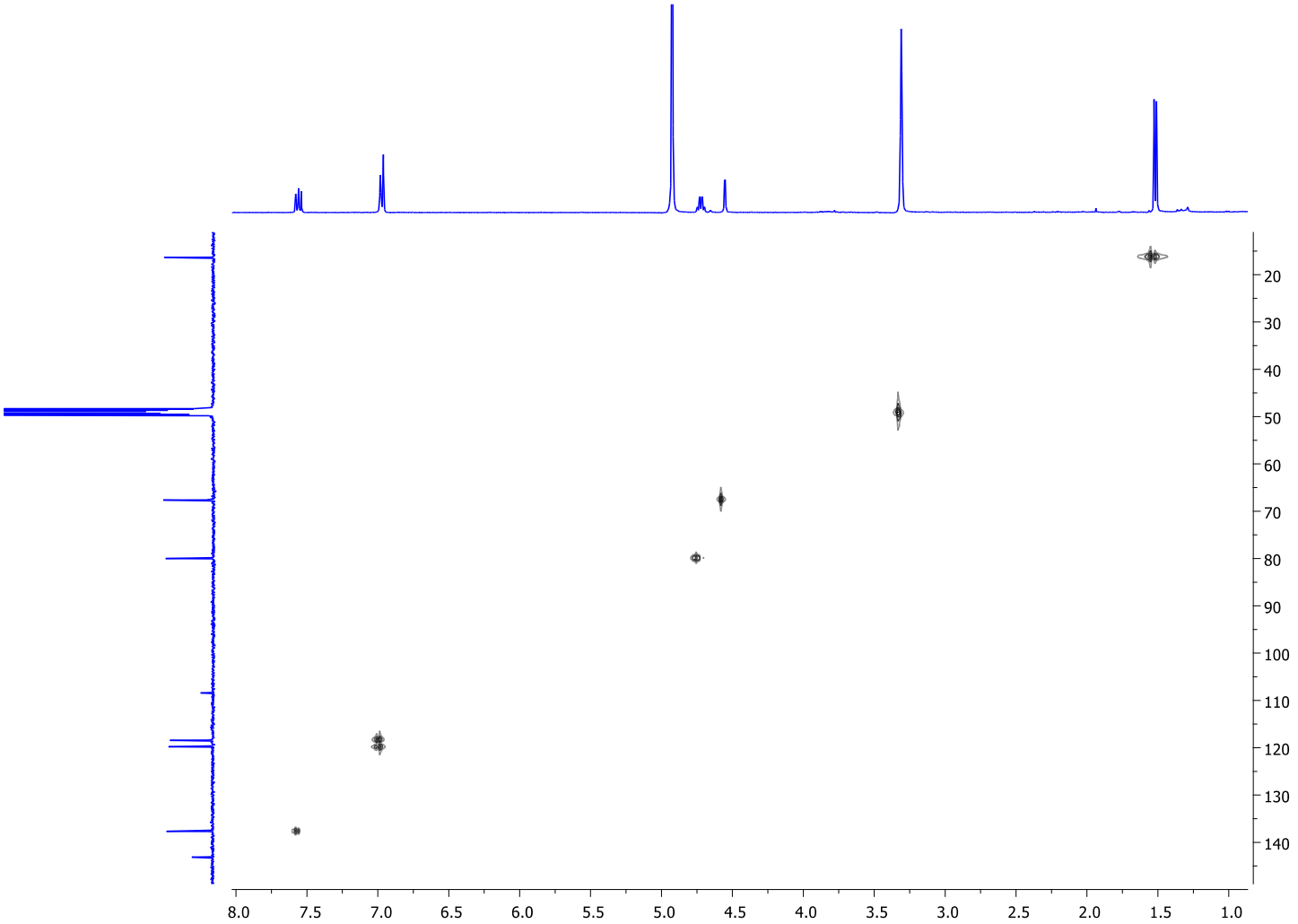

Figure S13. HSQC spectrum of compound **2** (CD_3OD).

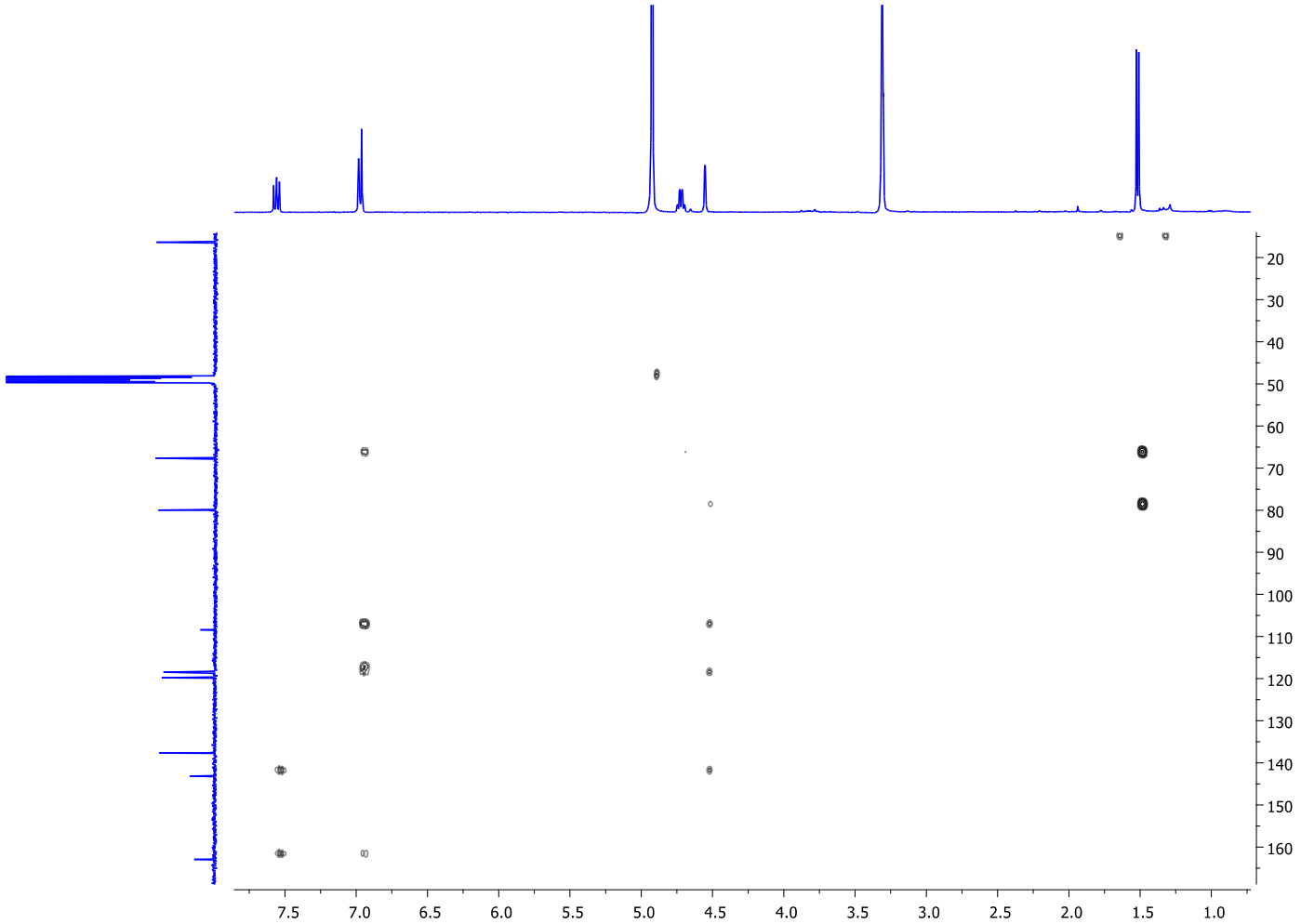

Figure S14. HMBC spectrum of compound **2** (CD_3OD).

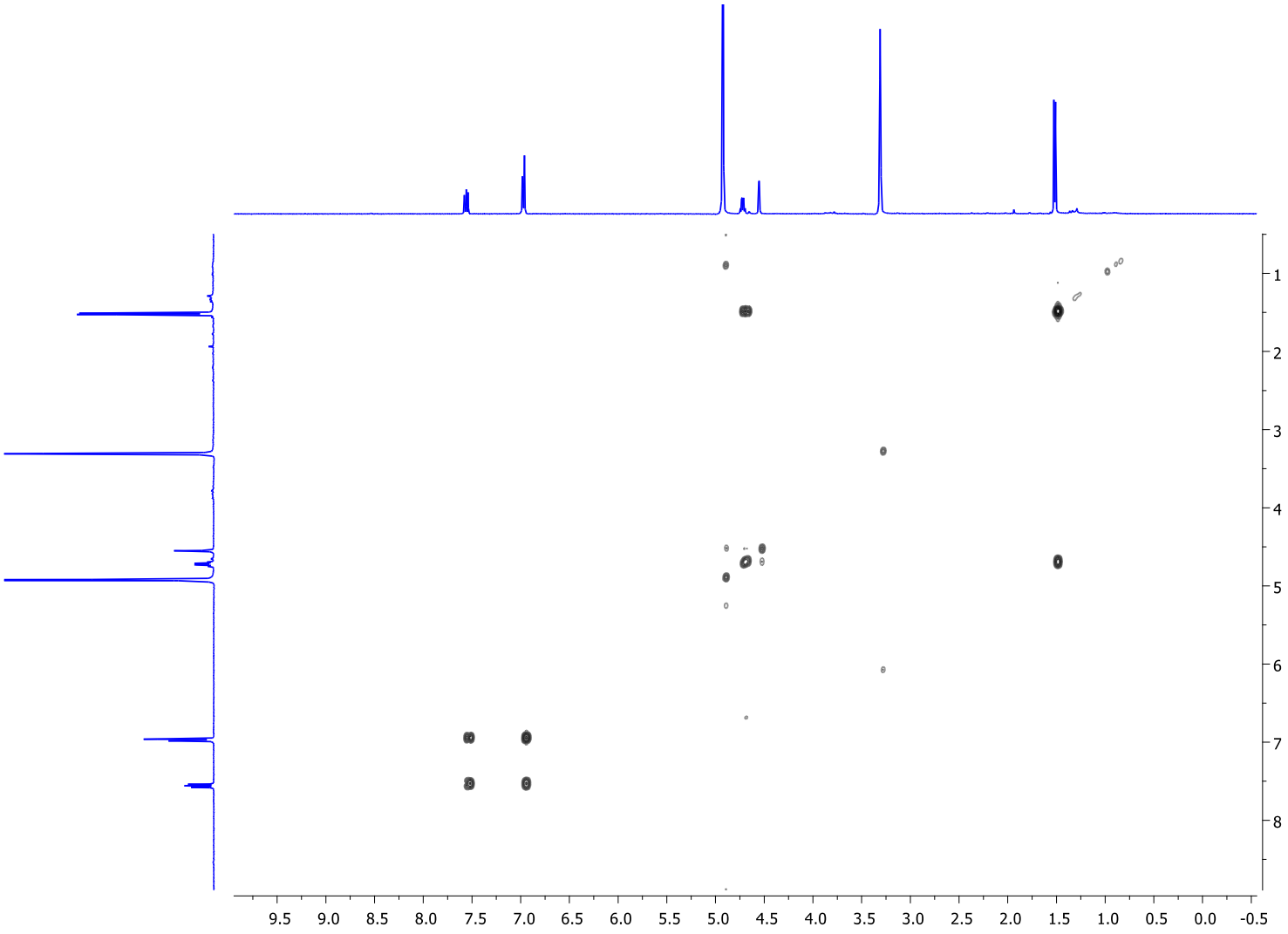

Figure S15. COSY spectrum of compound **2** (CD_3OD).

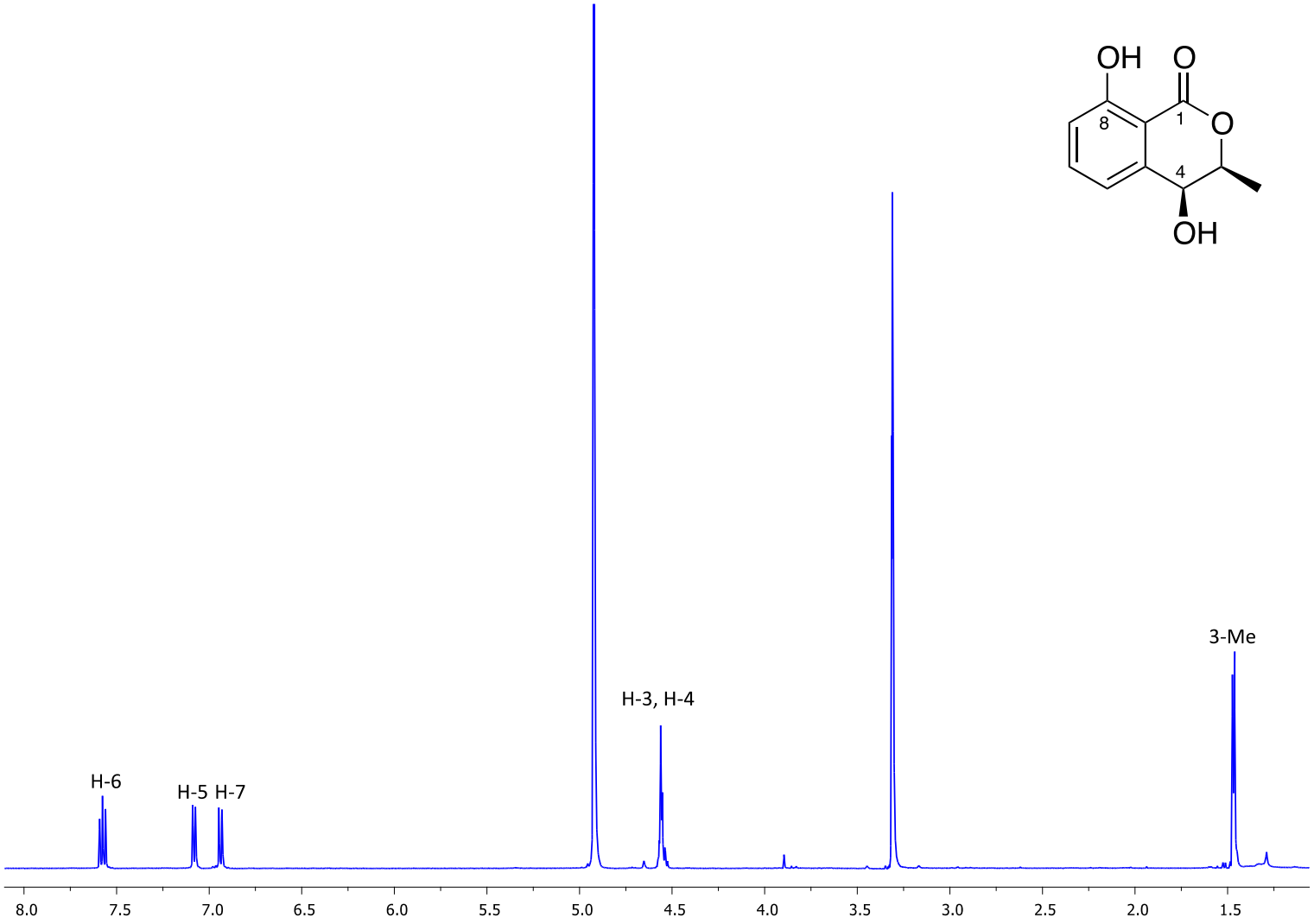

Figure S16. ^{1}H-NMR spectrum of compound **3** (500 MHz, CD_3OD).

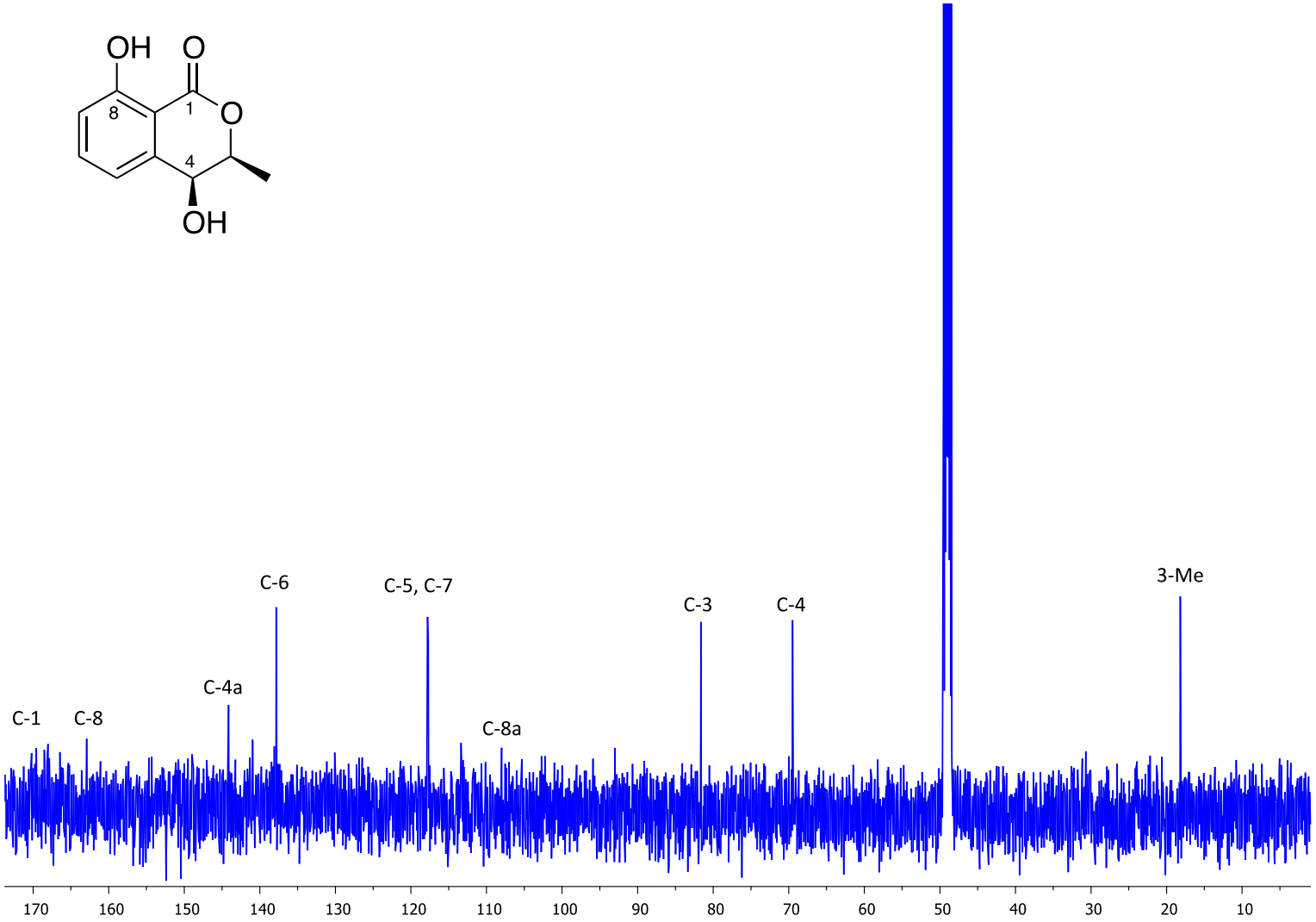

Figure S17. ^{13}C-NMR spectrum of compound **3** (125 MHz, CD_3OD).

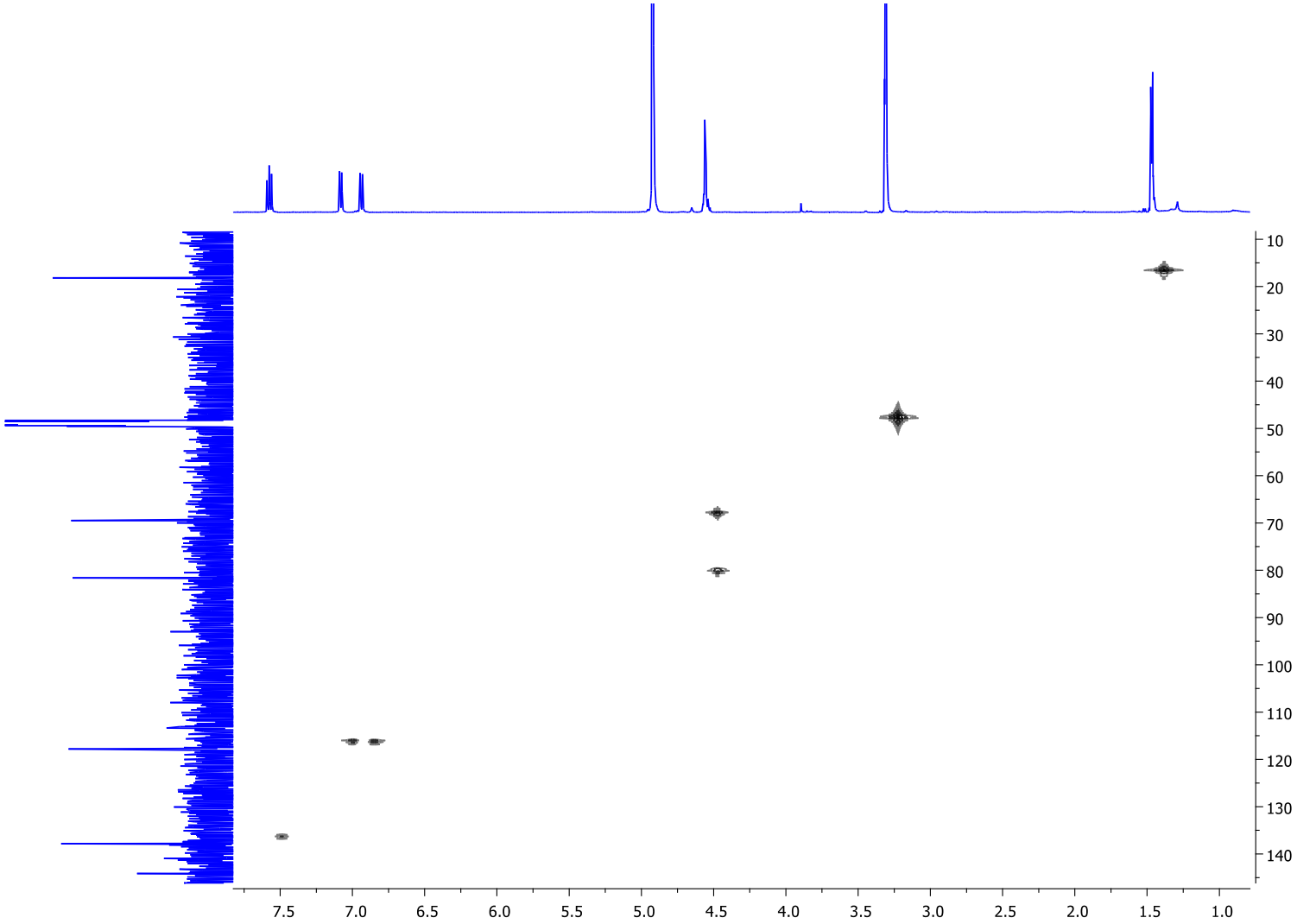

Figure S18. HSQC spectrum of compound **3** (CD_3OD).

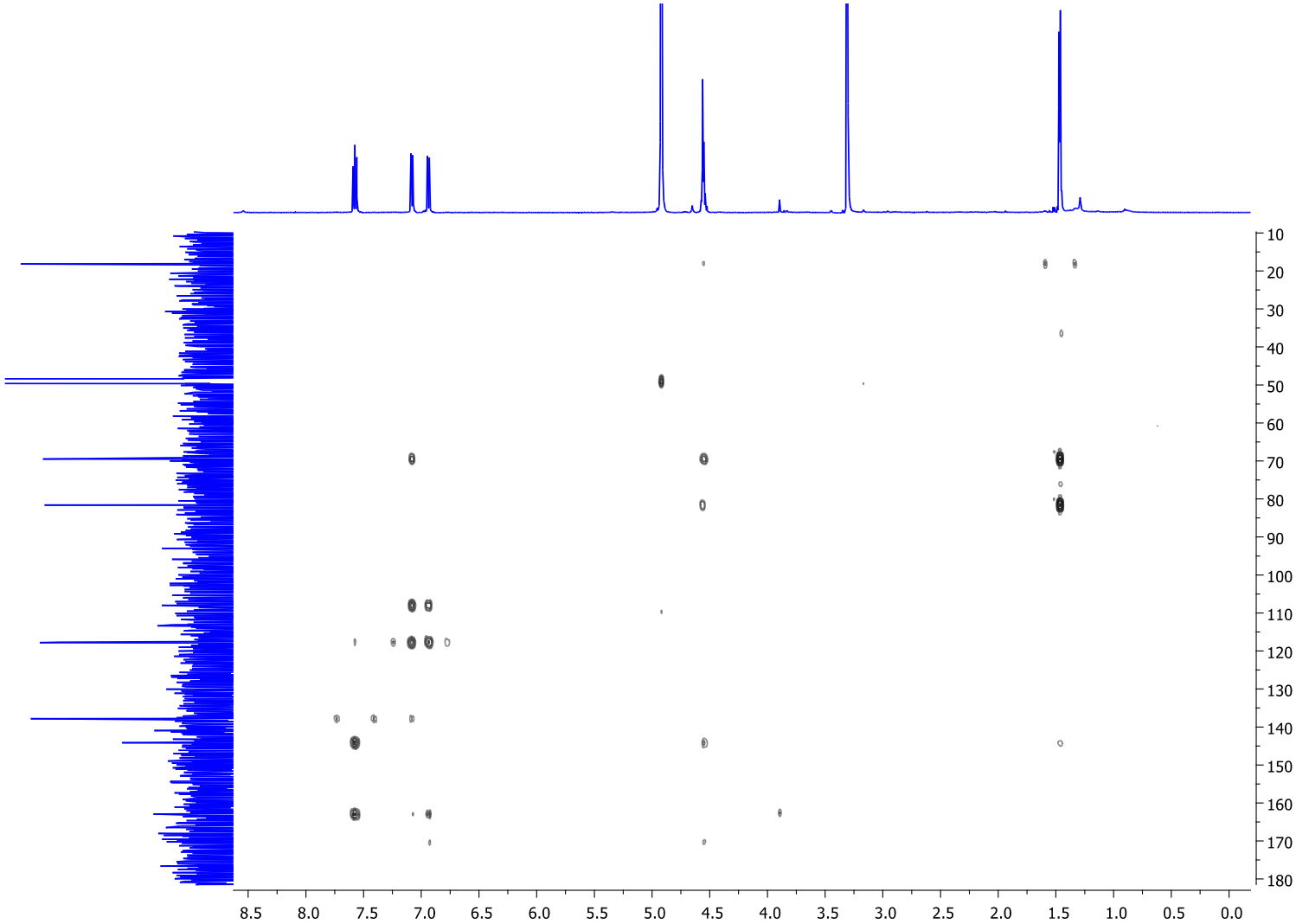

Figure S19. HMBC spectrum of compound **3** (CD_3OD).

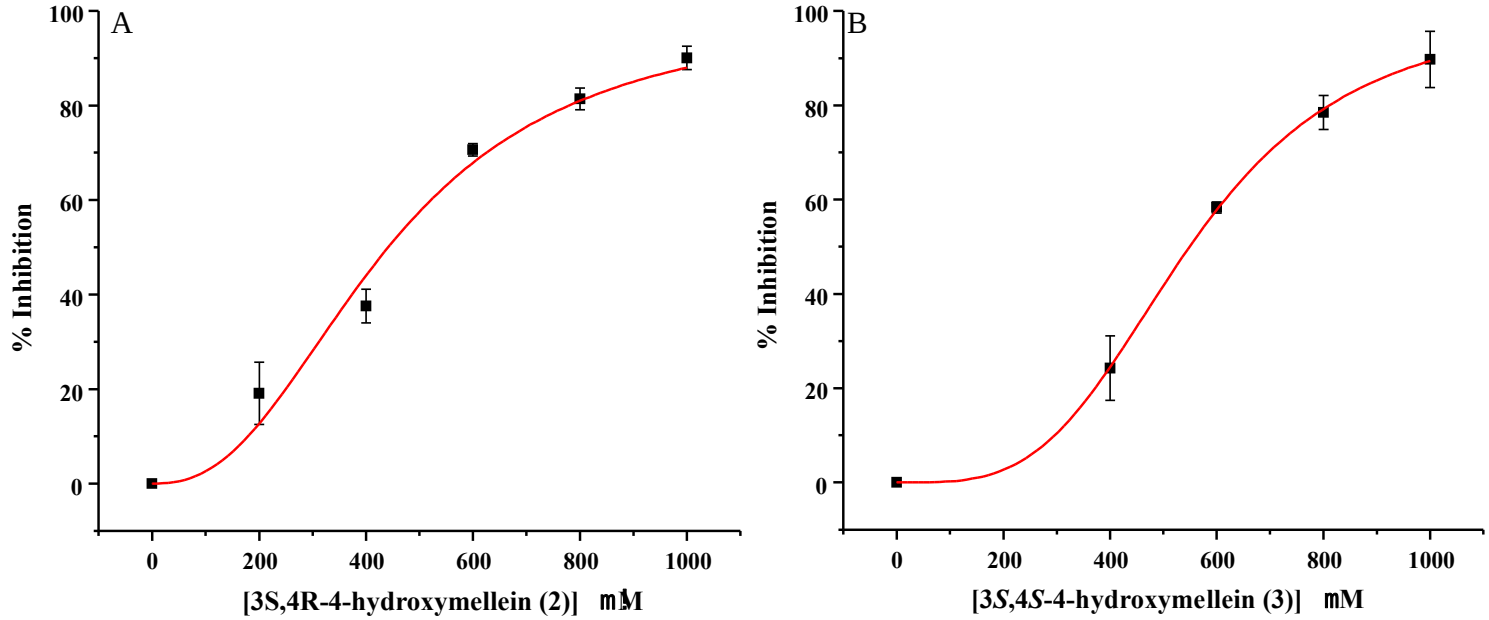

Figure S20. Enzymatic inhibitory activity of compounds **2** and **3** against *α*-glucosidase from *Saccharomyces cerevisiae* (*αGHY*; A and B respectively).

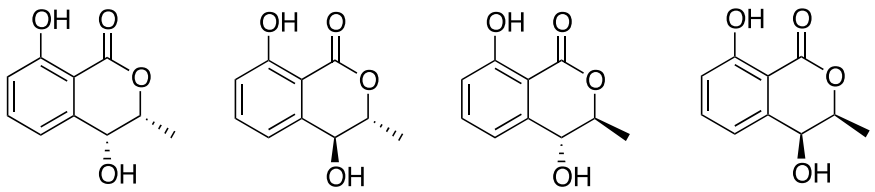

Figure S21. Four possible diastereoisomers of 4-hydroxymellein (**2**): **2a** 3*R*,4*R*; **2b** 3*R*,4*S*; **2c** 3*S*,4*R* and **3** 3*S*,4*S*.

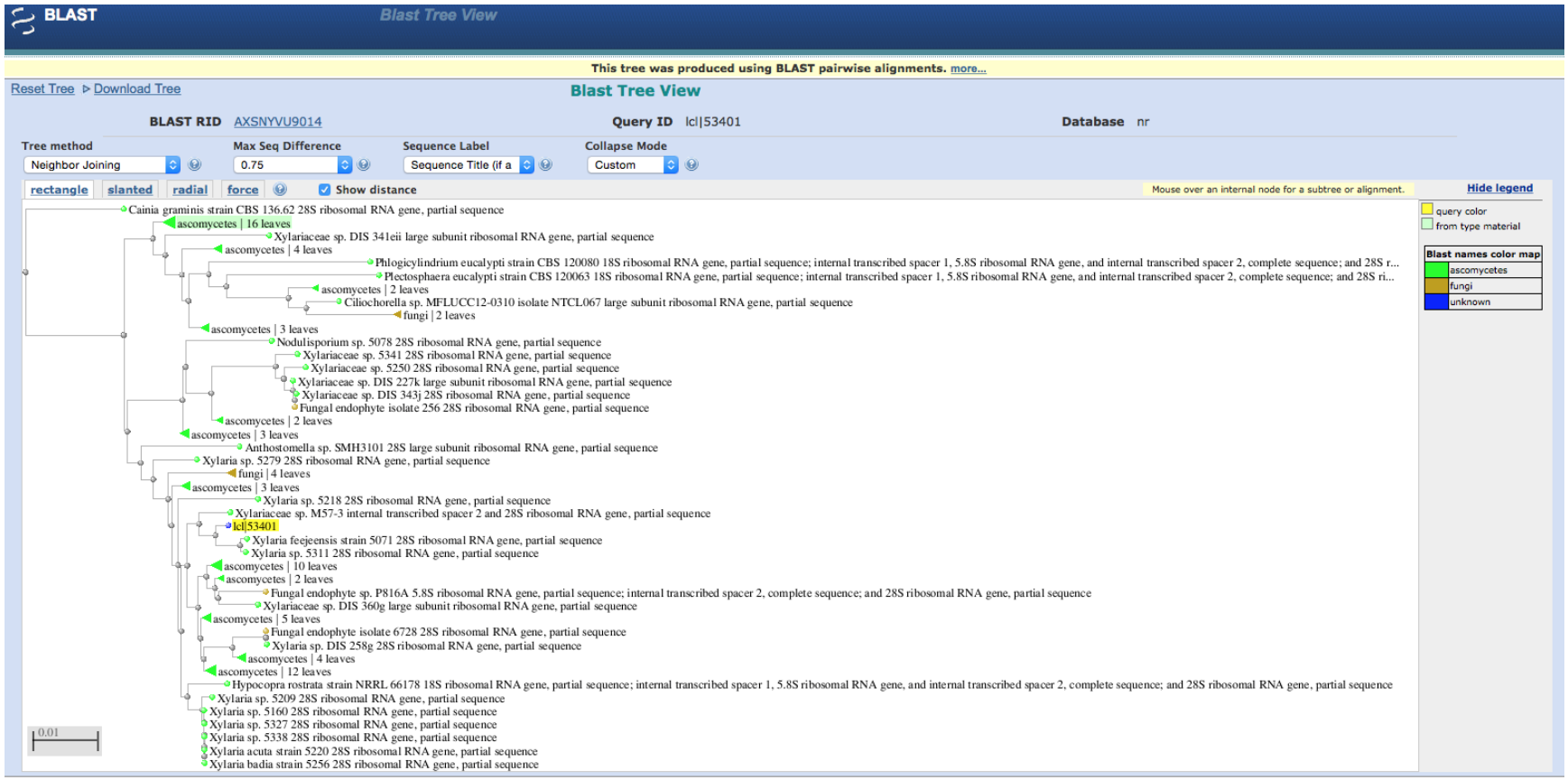

Figure S22. Distance phylogram based on BLAST of the 28S rRNA gene. The *H. latiflora* endophyte is the query (yellow highlight).

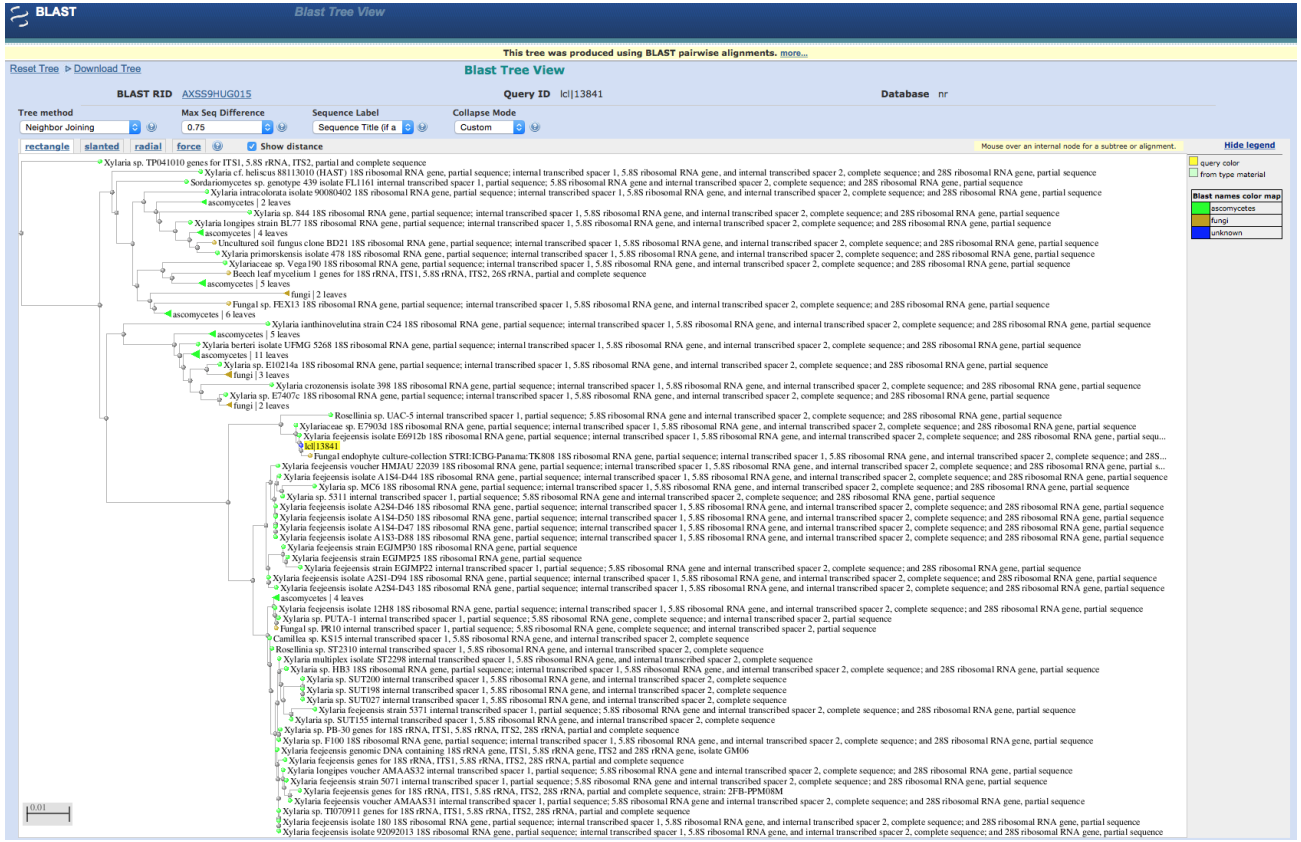

Figure S23. Distance phylogram based on blastn of the ITS region. The *H. latiflora* endophyte is the query (yellow highlight)